공학석사학위논문

Development of a Thermal Management System Model and a Capacity Fade Model for Li-ion Batteries in Electric Vehicles

전기차용 리튬 이온 배터리 열관리 시스템 모델 및 용량 저하 모델 개발

2013년 2월

서울대학교 대학원

기계항공공학부

최 종 우

Development of a Thermal Management System Model and a Capacity Fade Model for Li-ion Batteries in Electric Vehicles

전기차용 리튬 이온 배터리 열관리 시스템 모델 및 용량 저하 모델 개발

지도교수 차 석 원

이 논문을 공학석사 학위논문으로 제출함
2012년 10월

서울대학교 대학원
기계항공공학부
최 종 우

최종우의 공학석사 학위논문을 인준함
2012년 12월

위 원 장 _____ (인)

부위원장 _____ (인)

위 원 _____ (인)

Abstract

The thermal management system model for li-ion batteries in electric vehicles is developed. Convection heat transfer theories for the laminar and the turbulent flow are used. Both air cooled type and liquid cooled type thermal management systems are simulated and compared with experimental data. The open circuit voltage (OCV) and the ohmic resistance of the battery are given from experiments as map values indexed by the temperature and the state of charge (SOC). Constants for the activation loss are referenced from papers. Simulation results match well with experimental ones. The simulation model shows that finding efficient battery pack arrangement for the air cooled thermal management system is possible.

The general battery model with the capacity fade mechanism due to the SEI film generation is also developed. Simulation results show that the capacity fade of the battery depends on the temperature. By including the battery model with the capacity fade mechanism to the thermal management system model of the electric vehicle, it will be possible to find optimum control methods to increase the state of health (SOH) of the battery.

keywords : Lithium ion Battery, Electric Vehicle, Thermal Management System, Capacity Fade, State of Health

***Student Number* : 2011-20764**

Contents

List of Tables

List of Figures

1. Introduction

1.1. Overview

Due to the lack of oil and the environment pollution problem, electric vehicles become popular in these days. Electric vehicles, EVs, use electric power storage systems as their power sources. Batteries, supercapacitors, fuelcells and other kinds of electric power storage systems are used as main or assistant power sources of electric vehicles.

There are several kinds of electric vehicles; hybrid electric vehicle (HEV), plug-in hybrid vehicle (PHEV), fuelcell hybrid electric vehicle (FHEV) and so on. Although all of them use electric power for driving, there are several differences among them. Some of them use a battery only and others use a battery with other components like an engine. Some of them are charged directly using a plug and others use different methods like a regenerative brake.

To achieve high efficiency and safety, it is essential to use a power management system. The Power management system helps to choose a proper power source to use and the way that load is distributed to each power source. By adapting a proper power control logic to the management system, it is possible to achieve higher energy efficiency than that of a vehicle using engine as its only power source.

A type of EV that uses a battery as its only power source is chosen for the simulation model. Battery management system, BMS, is adapted as the power management system.

1.2. Objective of The Present Study

In this thesis, the thermal management system model and the capacity fade model for Li-ion batteries in EVs are developed and simulated.

Battery thermal management system (B-TMS) is a type of a management system belonging to BMS. B-TMS uses many components to control the battery temperature, which is related to the efficiency and the safety problem. While B-TMS is working, power is consumed at each component. Therefore, there exists a trade off between the battery safety and the power consumption of B-TMS. Modeling B-TMS would help identify effect of B-TMS and make an effective control logic for it.

With the efficiency and the safety problem, the total capacity of the battery becomes lower during cycling. Temperature, electric load, and many other conditions effect capacity fade of the battery. If the total capacity of the battery becomes so low that it is not suitable for EV, the battery has to be changed into a new one, which is directly related to the cost problem. Modeling battery capacity fade can help to identify decreasing of the capacity of the battery after driving. By using this information, it is possible to define an effective battery control method that minimizes the cost for the battery change.

2. Battery Thermal Management System

2.1. Battery Management System

Battery management system, BMS, is a system that helps safe and effective working of a battery. The battery pack adapted to an electric vehicle consists of battery modules and each battery module consists of battery cells of 15~30Ah capacity. For example, Chevrolet Volt, a plug-in hybrid vehicle, contains 288 Li-ion pouch cells connected as 3 parallel modules. The total capacity of the battery pack is 16kWh [1]. Nissan Leaf, a pure electric vehicle, contains 192 cells arranged as 48 modules. The total capacity is 24kWh. Since the battery pack in the EV consists of many battery cells, there exists possibility to distribute electric loads unevenly to each cell when BMS does not exist.

Voltage and internal resistance of the battery are affected by the remaining capacity of a cell. Heat generations at each cell are directly affected by electric loads. Therefore, uneven load distribution can decrease energy efficiency and make safety problems due to temperature.

The battery management system identifies voltage, state of charge (SOC), temperature, and other properties of each cell. By using input data, BMS does appropriate control to achieve high efficiency and safety. If SOC of one cell is to low, BMS makes electric load small which is headed for the cell. If battery temperature is to high, fan works to cool down the battery pack. It is possible to expect improvement in performance by defining a proper control logic to BMS.

2.2. Battery Thermal Management System

Battery thermal management system, B-TMS, is a part of BMS that controls temperature of a battery pack. Since the battery shows temporal or permanent performance degradation at high or low temperature [1-3], the role of B-TMS is important to maintain an optimum temperature range. Phenomena like thermal runaway or gas generation at high temperature can make the battery explode. Cold starting problem at low temperature can destroy internal structures of the battery cell. B-TMS uses many components to maintain the battery pack temperature in optimum range. It also makes to keep optimum temperature distribution among each cell.

Most electric vehicles of today use the battery thermal management system like an engine thermal management system of general vehicles. Simulation studies are also done under CFD or 1-D heat transfer model base [4-7].

There are two major types of the battery thermal management system.

2.2.1. Air Cooled Thermal Management System

Air cooled thermal management system simply uses a suction fan to cool down the battery temperature. It is used in vehicles like Sonata Hybrid and Nissan Leaf. The Suction fan makes ambient air flows through the battery pack. Convection heat transfer occurs between the air and the battery. Power consumption is low since it uses a fan as the only thermal management component. However, due to the same reason, the cooling effect is limited.

2.2.2. Liquid Cooled Thermal Management System

Liquid cooled thermal management system uses a pump to circulate liquid state coolant through the pipe that surrounds the battery pack. It is used in

vehicles like Chevrolet Volt and Ford Focus. Same as the air cooled thermal management system, convection heat transfer occurs between the coolant and the battery. Cooling effect is higher than that of the air cooled thermal management system because the thermal capacity of the liquid coolant is higher than that of the air. Power consumption is also higher since the pump consumes much power than the fan does.

It is possible to add optional components into both the air cooled and the liquid cooled thermal management system. A chiller is available for fast cooling. A heater is available to block the cold starting problem. A radiator can be used for heat transfer between the coolant and the ambient air. Many other components can be used. Adding components helps manage temperature more effectively but consumes much power. Air cooled TMS generally does not use other component to minimize energy consumption as well as to the low power consumption of the suction fan. However, liquid cooled TMS is frequently used with other components to maximize its cooling or heating effect. Since liquid cooled TMS uses a pump, a high power consumption device, to circulate coolant, it is possible to consume much power when the pump circulates coolant fast to accelerate convection heat transfer. By using additional components, the cooling speed becomes faster and power consumption at the pump becomes lower. When an appropriate control logic is adapted, total power consumption of the pump and additional components can be lower than that of the pump only.

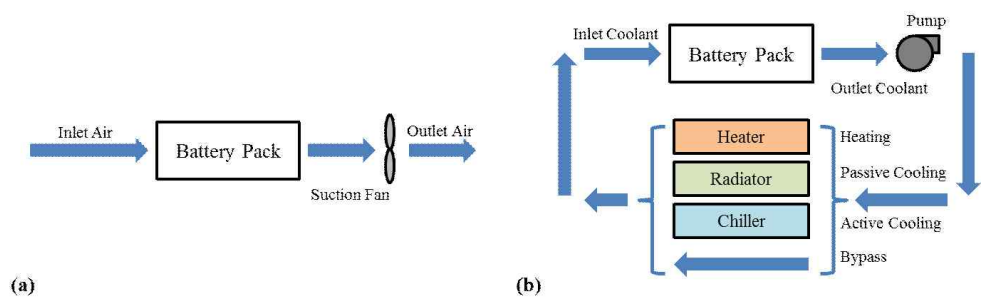

Figure 2.1. Schematic diagrams of (a) air cooled TMS (b) liquid cooled TMS

3. Battery Thermal Management System Simulation

3.1. Air Cooled TMS Model

3.1.1. Air Cooled TMS Overview

The schematic diagram of the air cooled thermal management system with the battery pack is shown in Figure 2.2. The arrangement of the total system used here is given from SK Innovation.

As mentioned in section 2.2.1, air cooled TMS uses the suction fan to make ambient air, which works as coolant, flowing through the battery pack. The battery pack consists of battery modules. And the battery module consists of battery cells. Modules in the battery pack are arranged as three columns. Air passes through each column sequentially. Convection heat transfer occurs between the battery and the air. Since the air is heated during passing through each column, the temperature of the air that goes into the third column is higher than one that goes into the first column. Therefore, the amount of heat transferred from each column to the air is different. Temperature of each column is also different from each other. To simulate these kinds of phenomena, thermal resistance method is used.

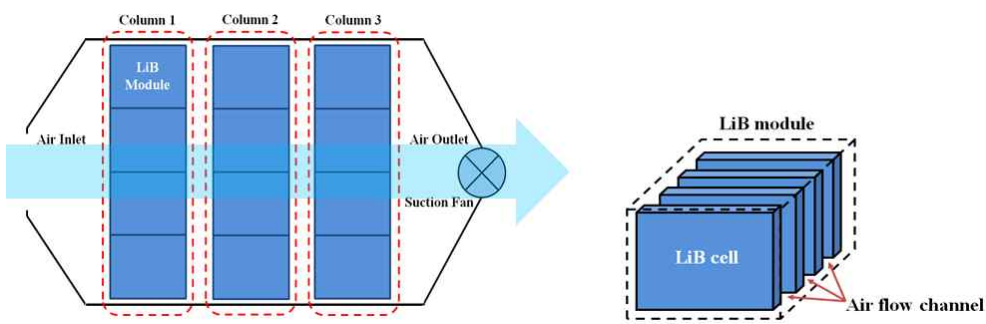

Figure 3.1. Detailed diagram of air cooled TMS

3.1.2. Heat Transfer Theory for Air Cooled TMS

Several assumptions are used to model air cooled TMS. Firstly, heat transfer is only possible between the cell and the air that passes through the battery pack. In a real case, heat transfer is also possible between the battery pack and the chassis, the air in the upside or downside of the battery pack and so on. However, it is hard to model those kinds of phenomena. Additionally, the amount of heat transferred to them is small compared to the forced convection heat transfer.
Secondly, time consumption for coolant flow is neglected. The inlet air changes into the outlet air with modified temperature during only one timestep in simulation model. It can be a problem when the battery pack is so long that time consumption inside of the battery pack is significant. Cooling speed would be much faster than that of the real case. However, the length of the battery pack used here is not that long and the cooling speed is so fast that it is possible to neglect the time consumption inside of the battery pack. Same assumption is also used in liquid cooled TMS model and becomes a problem in that case. It is explained in section 3.2.

Thermal resistance method and lumped capacitance method are used to simulate the heat transfer mechanism of air cooled thermal management system. Heat transfer between the battery and the air can be separated into conduction and convection heat transfer. The effect of radiation heat transfer is negligible. Conduction heat transfer occurs from the high temperature cell to the case. The battery case is made with aluminium, metal that has good thermal conductivity. By using aluminum case with pouch cell, it is possible to provide even temperature distribution in whole battery cell surface.
Convection heat transfer occurs from the battery case to the air. Constants that are needed for simulation are referred from material value.

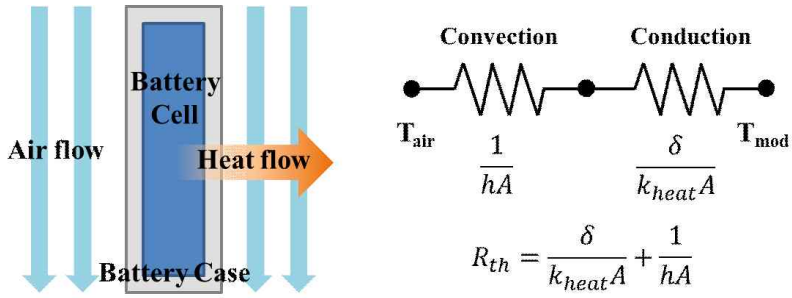

Figure 3.2. Thermal resistance method for heat transfer at battery cell

Table 3.1. Material Properties for air cooled TMS [8]

	Density ρ (kg/m^3)	Specific Heat c_p (J/kg·K)	Kinetic Viscosity ν (m^2/s)	Thermal Conductivity k (W/m·K)	Prandtl Number Pr
Battery Cell	-	1133	-	-	-
Aluminium	-	-	-	237	-
Air (300K)	1.1614	1007	1.589×10^{-5}	2.63×10^{-2}	0.707

Heat transfer coefficient h for convection heat transfer is calculated from Nusselt number equation. The internal flow for a noncircular pipe is assumed since air flows through the gap between battery cell. If the air flows only at the boundary surface of each battery module, the external air flow has to be assumed. Nusselt number equations for the internal type and the external type flow are different. Therefore, defining a correct flow type is important to model convection heat transfer.

In this internal flow model, speeds of the air that passes through each gap between cells at the same column are assumed to be same. It means that speed change due to the friction with the wall does not exist. Therefore, the speed of the air is calculated by dividing the total volumetric air flow into the total cross sectional gap area between cells. If each gap size is same, the amount of the air that flows through the each gap also becomes same.

In this case, the heat transfer phenomenon becomes same for all cells in the same column because convection heat transfer coefficient depends on the speed of the coolant. By modeling heat transfer of one cell in each column, it is possible to predict temperature of all cells in the same column.

Reynolds number becomes a reference value to separate the laminar and the turbulent flow region. Hydraulic diameter is used as a length value for the internal flow. For the internal flow, when Reynolds number is lower than 2300, the flow is classified as laminar one. The flow is classified as turbulent one when Reynolds number is higher than 4000. If the hydraulic diameter is fixed, velocity of the flow does not affect much to the Nusselt number in the laminar flow case. Nusselt number values for fully developed internal laminar flow are arranged as table. Compared with the laminar flow case, Nusselt number of the fully developed internal turbulent flow is directly affected by the value of the Reynolds number, which is associated with flow velocity. The following equations explain fully developed internal turbulent and laminar flow [8].

$$D_h = \frac{4ab}{2(a+b)} \tag{3.1}$$

$$Re_D = \frac{vD}{\nu} \tag{3.2}$$

$$Nu_D = \frac{hD}{k} \tag{3.3}$$

Laminar flow, fully developed, uniform surface temperature

Table 3.2. Nusselt number for fully developed laminar flow

Cross Section						
b/a	-	1.0	2.0	4.0	8.0	∞
Nu_D	3.66	2.98	3.39	4.44	5.60	7.54
$f\,Re_D$	64	57	62	73	82	96

Turbulent flow, fully developed

$$f = (0.790 \ln Re_D - 1.64)^{-2} \tag{3.4}$$

$$Nu_D = \frac{(f/8)(Re_D - 1000)Pr}{1 + 12.7(f/8)^{1/2}(Pr^{2/3} - 1)} \tag{3.5}$$

Modeling forced convection heat transfer is possible by using the above equations about the heat transfer coefficient. However, there exists difficulty to calculate the convection heat transfer coefficient for natural convection. Although fan is not working, the convection heat transfer occurs because of the air flow occurred by temperature deference. Density change by the temperature makes the natural air flow and the convection heat transfer occurs. There are some equations that explain natural convection heat transfer coefficient. However, in this case, convection heat transfer occurs inside of the small gap between battery cells. Direction of the total air flow by the natural convection has to be a length direction. Therefore, the equations about the general natural convection [8] can not be adapted.

General natural convection, within parallel vertical plates, thin gap

$$Gr_S = \frac{g\beta(T_s - T_\infty)S^3}{\nu^2} \tag{3.6}$$

$$Ra_S = Gr_S Pr \tag{3.7}$$

$$Nu_S = \frac{Ra_S(S/L)}{24} \tag{3.8}$$

To simulate the natural convection heat transfer between the battery and the air, the heat transfer coefficient is calculated as the fitting value. The heat transfer coefficient of general natural convection is directly proportional to the temperature difference between an object and the air. Following this relationship, multiplying fitting constant to the temperature difference is used as the natural convection heat transfer coefficient.

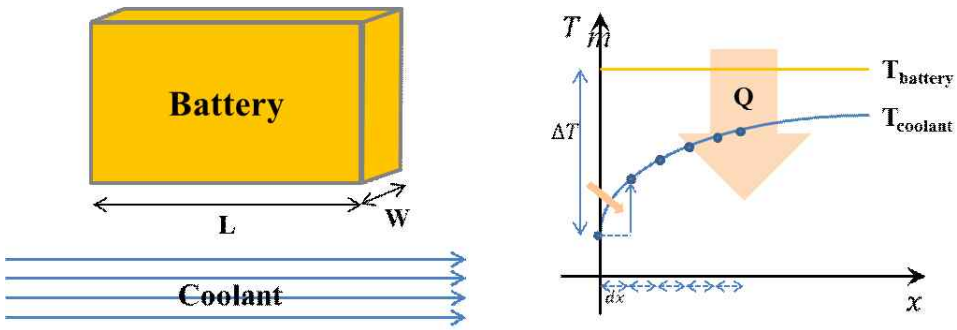

Figure 3.3. Heat transfer mechanism between battery and coolant

Using the convection heat transfer equations, the heat transfer model using thermal resistance method can be made. It is assumed that there is no temperature gradient inside of the each battery cell. Aluminium battery case that surrounds battery cell helps conduction heat transfer, which makes even temperature distribution at the whole surface of each cell. By using this assumption, the constant surface temperature condition of cells at each timestep is adaptable.

At each timestep, the surface temperature of each cell is constant value, which means no temperature gradient exists. When the coolant passes by the cell surface, heat transfer occurs between the cell and the coolant.

$$\dot{m}c_{p,cool}dT_{cool} = \frac{T_{bat} - T_{cool}}{AR_{th}}dA = \frac{T_{bat} - T_{cool}}{AR_{th}}(Wdx) \tag{3.9}$$

The temperature of the coolant changes during flowing because of the heat transfer. If the temperature of the battery is higher than the coolant, the outlet temperature of the coolant becomes higher than the inlet temperature.

$$\int_{T_{in}}^{T_{out}} \frac{dT_{cool}}{T_{bat} - T_{cool}} = \int_{0}^{L} \frac{Wdx}{\dot{m}c_{p,cool}AR_{th}} \tag{3.10}$$

$$T_{out} = T_{bat} - (T_{bat} - T_{in})\exp\left(-\frac{A}{\dot{m}c_{p,cool}AR_{th}}\right) = T_{bat} - (T_{bat} - T_{in})\exp\left(-\frac{1}{\dot{m}c_{p,cool}R_{th}}\right) \quad (3.11)$$

The amount of the heat transferred to the coolant is same as that of the heat transferred from the battery cell.

$$Q = \dot{m}c_{p,cool}(T_{out} - T_{in}) \quad (3.12)$$

Therefore, by calculating the transferred heat, the temperature change of the battery cell during each timestep can be calculated.

$$Q\,dt = m_{bat}c_{p,bat}(T_{bat,current} - T_{bat,next}) \quad (3.13)$$

$$\therefore T_{bat} = T_{bat,init} - \int_0^t \frac{Q}{m_{bat}c_{p,bat}}dt = T_{bat,init} - \int_0^t \frac{\dot{m}c_{p,cool}(T_{out} - T_{in})}{m_{bat}c_{p,bat}}dt \quad (3.14)$$

3.1.3. Simple Battery Model

To calculate a heat generation and voltage of a battery pack, simple battery model based on the single particle model is developed. This model is used to model battery packs in both the air cooled and the liquid cooled thermal management systems.

During charging and discharging, the lithium ion inside of the battery moves from one electrode to another. The electric potential of each electrode changes with lithium ion concentration. The potential difference between negative and positive electrode becomes open circuit voltage of the battery.

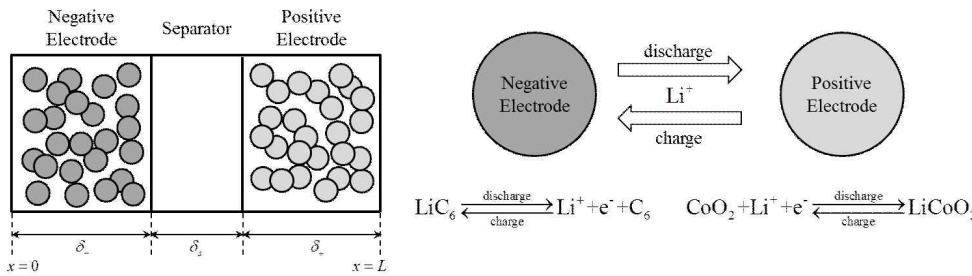

Figure 3.4. Internal reaction of $LiCoO_2/LiC_6$ lithium ion battery

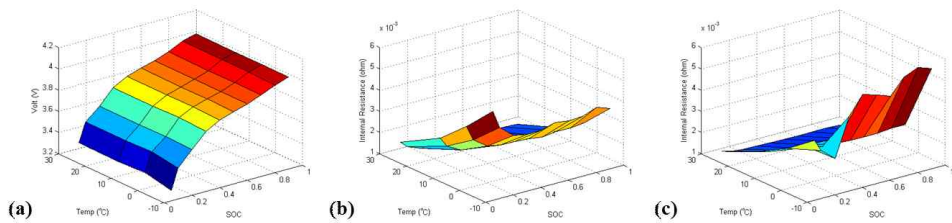

Figure 3.5. Temperature and SOC dependencies of (a) OCV
(b) internal resistance (discharge) (c) internal resistance (charge)

With OCV change due to concentration, voltage loss exists during battery working. There are two major reasons of the voltage loss. To make reactions that enables current flow possible, a part of the electric potential has to be used. This loss is called the electrochemical voltage loss. Another one is the ohmic voltage loss that is caused by electric resistance of the battery itself.

The voltage loss of the battery increases as the current load increases. Temperature also affects OCV and voltage loss. Experimental OCV and internal resistance map data sorted by temperature and concentration are used for the simple battery model. The electrochemical voltage loss is developed by using Butler-Volmer equation. Transfer of ion because of diffusion is neglected to improve simulation time. State of concentration is used instead of surface concentration ratio. Detailed explanation about battery model is presented in the later section.

$$i = i_0\left\{\exp(\frac{\alpha nF\eta}{RT}) - \exp(-\frac{(1-\alpha)nF\eta}{RT})\right\} \quad (3.15)$$

$$V = OCV - iR_{int} - \eta \quad (3.16)$$

A heat generation of the battery is assumed same as the energy loss due to the voltage loss. The voltage loss of the battery means energy disappears during working. This loss of energy has to be changed into other kinds of energies like heat, sound, light and so on. Here, it is assumed that all of the energy loss due to the voltage loss changes into heat. The heat generation of each battery cell can be calculated by using this assumption.

$$Q_{gen} = I \times (OCV - V) \quad (3.17)$$

3.1.4. Experimental and Simulated Results

Three experimental results for different conditions are given from SK Innovation. Arrangement of the battery pack and the air thermal management system is explained in section 3.1.1. Each data contains voltage and temperature data tested under charging/discharging current load with TMS working or non-working condition. All experiments are done with the battery pack only, not with the vehicle. Properties of the battery pack and the air cooled thermal management system are arranged as a table.

Table 3.3. Properties for air cooled TMS model

Battery Cell		50Ah, 1.41kg
Arrangement	1st column	4 modules, 6 cells in each module
	2nd column	4 modules, 6 cells in each module
	3rd column	4 modules, 10 cells in each module
Suction Fan		$120 m^3/h$, 12V, 4A (Nominal)

The first experiment was done under TMS working condition. Battery is charged and then discharged. Temperature goes up during working time due to the heat generation. Forced convection makes the battery temperature down fast. Since each column has different temperature, maximum and minimum temperature of the battery pack are simulated. The third column has the highest temperature since the heat transfers to the air during passing through first and second column. Therefore, inlet coolant temperature becomes high for third column compared with those of the first and the second column. Room temperature is used as the first column inlet coolant

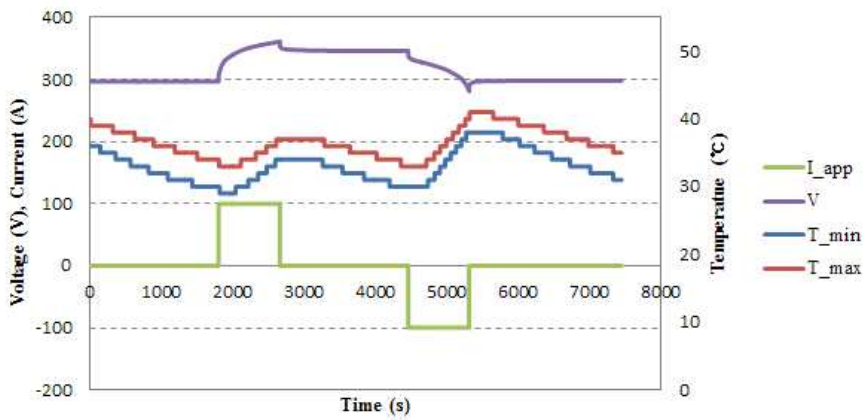

Figure 3.6. Experimental data under fan on condition, charging-discharging load temperature.

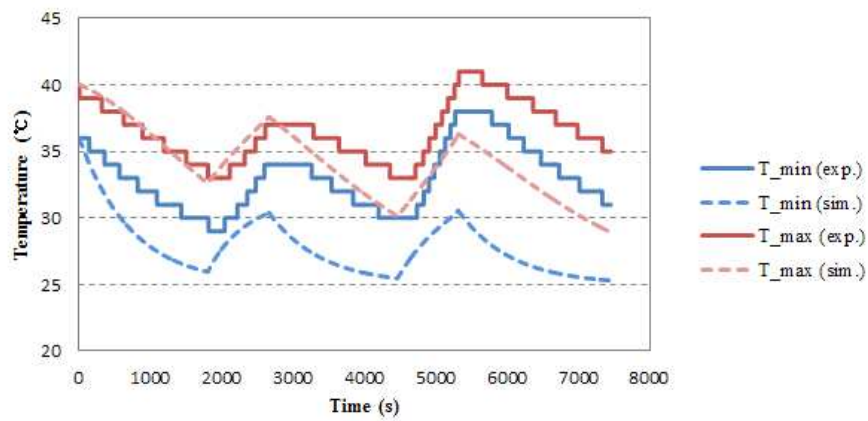

Figure 3.7. Error between experimental and simulated temperature data

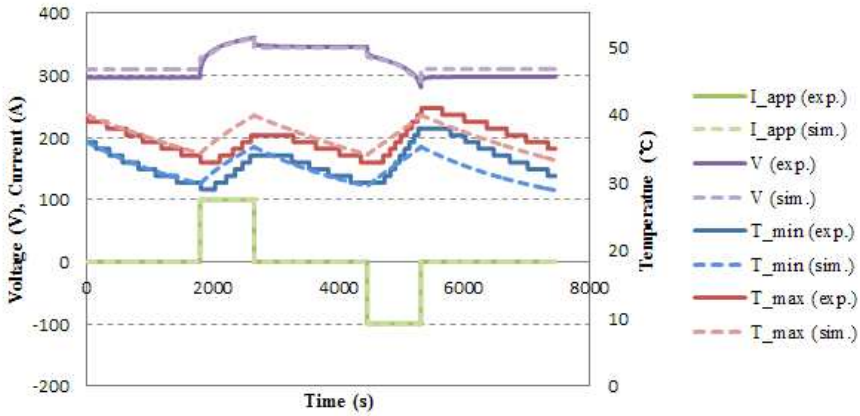

Figure 3.8. Simulation data with fitting factor for heat transfer coefficient

There is a significant difference between the experimental result and the simulation result. Cooling effect of air cooled TMS is much higher in the simulation result. Fitting factor for the heat transfer coefficient is adapted to remedy this error. After fitting factor is used, the average differences between the simulated and the experimental temperature are ±1.49℃ for both maximum temperature and minimum temperature. Maximum differences are +3.99℃ and −4.69℃. Compared with simulated temperature and experimental temperature, there is a time gap before the temperature rises. Temperature starts to rise about 300s faster in the simulation. This time gap is generated from the assumption about no time consumption in section 3.1.2. Error in the temperature will be decreased after adding this time consumption to the simulation model.

The voltage difference is average 7.74V and maximum 21.6V, 7.20% of the total pack voltage. It is high under no current condition. It means that an error exists in open circuit voltage data inserted to the simulation model. To modify this error, OCV map has to be updated.

The second experiment was done under TMS non-working condition. Battery is charged and then discharged. Average temperature differences are ±1.17℃ and ±1.02℃. The time gap between the simulated and the experimental temperature also exists. The temperature difference becomes bigger after 4100s. The current is zero after 3500s. Natural convection heat transfer occurs in this section. Compared with the natural heat transfer under no current condition from 1000s to 2700s, decreasing temperature after 4100s is too fast. Therefore, it is possible to assume that there is an experimental error after 4100s. The simulated result and the experimental result match well except this section.

The last experiment was done a long time under TMS non-working condition. Battery is only charged shortly at the first time. The average temperature differences are ±0.707℃ and ±0.787℃. Although the fitting factor is used for the natural heat convection, the tendency of the temperature change matches well between the experimental data and the simulation data.

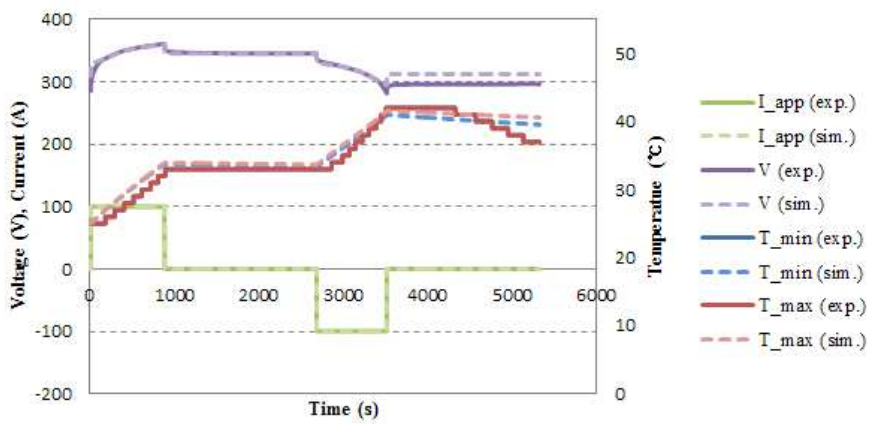

Figure 3.9. Simulation data under fan off condition, charging-discharging load

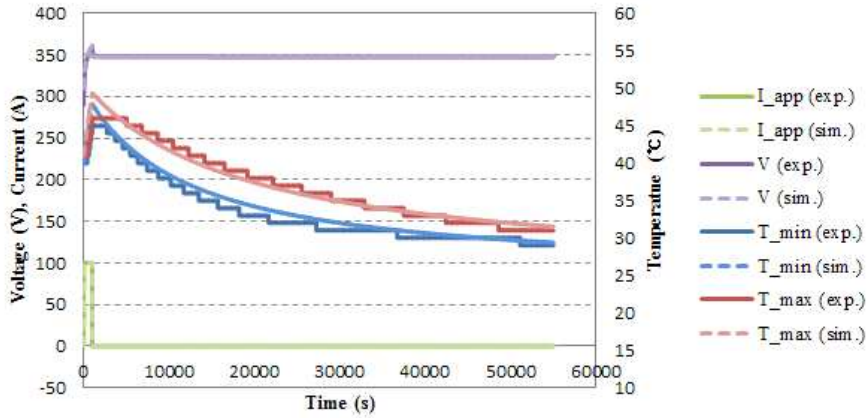

Figure 3.10. Simulation data under fan off condition, short charging load

3.1.5. Further Simulation about Pack Arrangement

The battery pack used for validation at section 3.1.4 is arranged as 3 columns. Each column has 4 modules. Each module consists of 6 or 10 battery cells. Due to the difference between the number of cells in each module, the arrangement of the battery pack can affect battery temperature. A module with many battery cells generates more heat compared with others. If gap size between cells is same as those of all modules, the total cross sectional area for column with many cells will be larger than those for other columns. Since volumetric air flow is conserved, the air speed and the convection heat transfer become lower.

To show an effect of the pack arrangement, modules that consist of 4, 6, 8 cells are assumed for simulation. The battery pack is arranged as three columns. Each column has 4 modules of same type. Other properties of the battery pack, the cell and the thermal management system are same with the above simulation. The ambient temperature is set to be 25℃. The initial

temperature of each cell is same as the ambient temperature. Fan on condition under charging-discharging load is chosen. Pack is charged and then discharged 3 times with 80A. The period of each current load is 1000s. 2000s rest time exists between each current load. Initial SOC is 0.1.

Figure 3.11 shows the simulation results under 4-6-8 arrangement and 8-6-4 arrangement. In 4-6-8 arrangement, the first column has 4 modules that consist of 4 cells. The last column has 4 modules that consist of 8 cells. The temperature difference exists due to different arrangements. Voltage is almost same for two simulations because of the same current loading and the similar temperature values. It can be known from the simulation that 8-6-4 arrangement is better than 4-6-8 arrangement. Although the lowest temperature is higher, both the maximum temperature and the difference between the maximum and the minimum temperature are low in 8-6-4 arrangement. Because of the inlet coolant temperature, cooling effect of the first column is higher than that of the last column. Therefore, by arranging a column that has the most cells to the front, total temperature distribution of the battery pack can be improved.

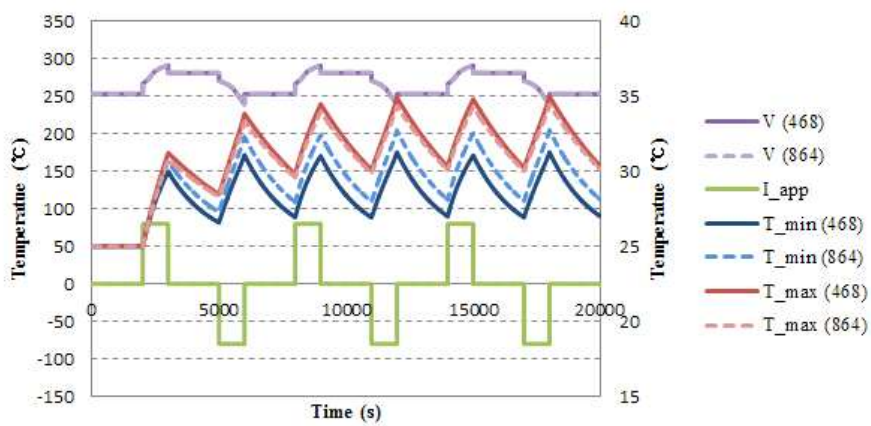

Figure 3.11. Simulation data under fan on condition, 4-6-8 and 8-6-4 arrangement

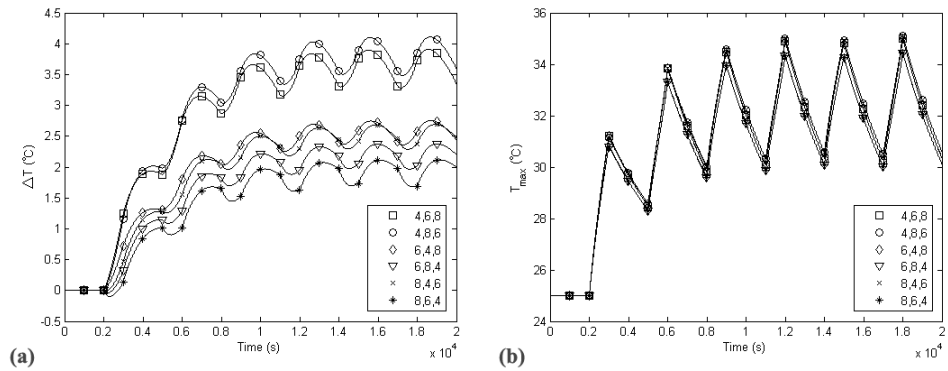

Figure 3.12. (a) Temperature difference (b) Maximum temperature by different pack arrangements (1)

Figure 3.12 shows the temperature differences and the maximum temperatures of the battery pack for each pack arrangement. As mentioned above, 8-6-4 arrangement has the lowest temperature difference, maximum ＋2.1173℃. The highest temperature difference occurs at 4-8-6 arrangement, maximum ＋4.1085℃. The maximum temperatures of each arrangement are almost same. 4-8-6 arrangement has the highest maximum temperature and 6,8,4 or 8-6-4 arrangement has the lowest maximum temperature. However, the differences between the maximum temperatures are only 0.5℃ range. Considering both the temperature difference and the maximum temperature, it is possible to say that 8-6-4 arrangement is the best arrangement method among 6 arrangement methods.

There are other ways to arrange the total battery cells in three column. 10-4-4, 12-4-2, 13-3-2, 16-1-1 arrangement are also simulated. Temperature of the first column becomes higher than the third column in the last three cases. These results comes from the large heat generation and the lack of heat transfer due to many cells in the first column. Compared to 8-6-4 arrangement, the maximum temperature is decreased by 1℃. The temperature

difference is also decreased. The simulation shows that 12-4-2 arrangement is the best battery pack arrangement. The maximum temperature difference is only 0.8981℃ and the maximum temperature is 33.3644℃, 1.5℃ lower than that of 4-8-6 arrangement. Like this case, the arrangement of the battery pack affects the temperature a lot in serial air cooled thermal management system. Simulation can help to choose the best pack arrangement that minimizes the temperature difference and the maximum temperature.

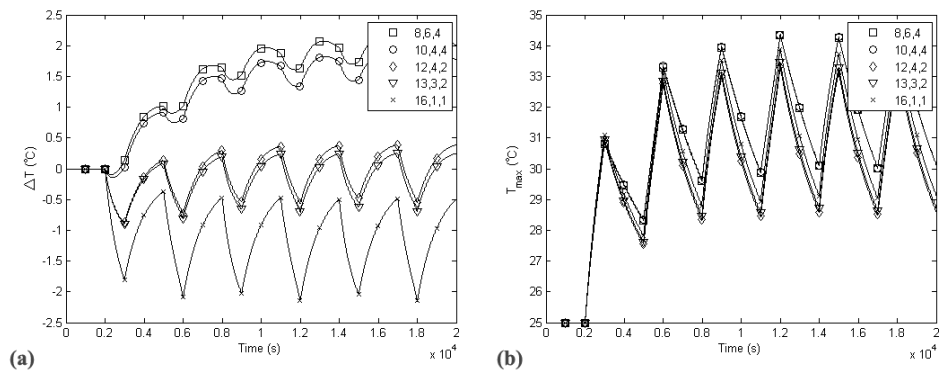

Figure 3.13. (a) Temperature difference (b) Maximum temperature by different pack arrangements (2)

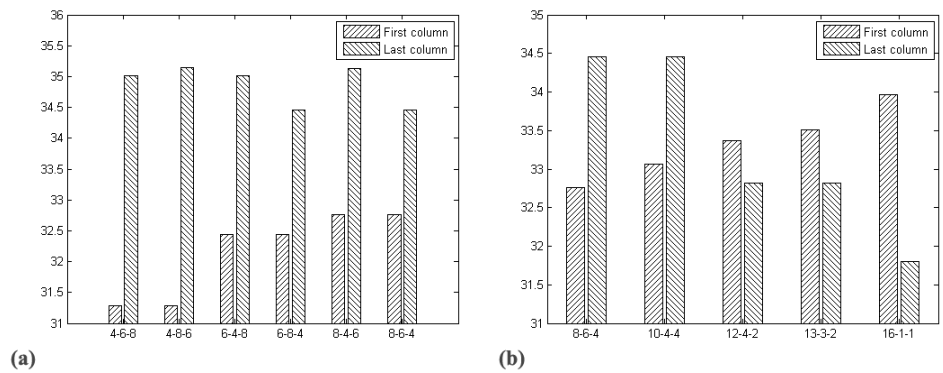

Figure 3.14. Maximum and minimum temperatures of (a) 4,6,8 base arrangements (b) other arrangements

3.2. Liquid Cooled TMS Model

3.2.1. Liquid Cooled TMS Overview

The schematic diagram of the liquid cooled thermal management system with the battery pack is shown in Figure 3.14. The arrangement of the total system used here is the one that is embedded in the GM Volt [1,9]. To compare simulation data with real ones, GM Volt liquid cooled thermal management system is chosen and tested.

50:50 mixture of deionized water and DEX-COOL^{TM} engine coolant is used as the coolant of the liquid cooled thermal management system in GM Volt [10]. Liquid state coolant circulates through the pipe that surrounds the battery pack. Each cooling fin is located between two battery cells. Coolant in the inlet pipe goes into the outlet pipe by passing through fins between the battery cells. Heat transfer occurs between the battery cell and the coolant which passes through the fins. Since the inlet coolant parallelly passes through all fins at the same time, heat transfer phenomenon becomes same for all cells in the battery pack. It is different from air cooled TMS modeled in section 3.1, which coolant passes through each cell serially.

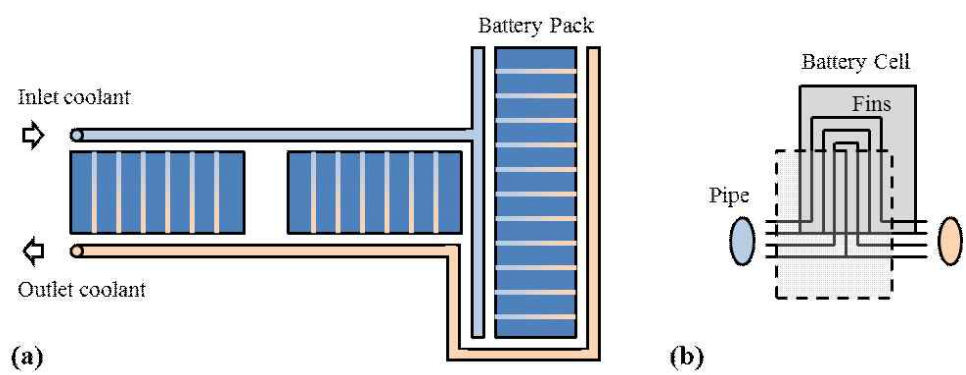

Figure 3.15. Detailed diagram of liquid cooled TMS
(a) total battery pack (b) each cell

3.2.2. Control Logic for Liquid Cooled TMS

As mentioned in section 2.2.2, many components are used in liquid cooled thermal management system. Pump, heater, radiator and chiller are used in GM Volt liquid cooled TMS. Working modes are categorized as four sections [10,11]. Each mode uses different cooling and heating components. Mode change is based on the battery temperature.

During driving, the temperature of the battery pack in electric vehicle is preferred to be kept in optimum range. When temperature goes too low, the speed of the electrochemical reactions inside of the battery cell becomes slower. Since the current flow is directly related with lithium ion transfer inside of the battery cell, slow reaction makes battery power limited. This situation, known as a cold starting problem, often happens in cold weather. When a battery is cooled during parking, available power becomes lower than motor starting limit. On the other hand, when the temperature goes too high, safety problem arises. Unwanted internal reactions like gas generation and self decomposition are possible in high temperature. Although working at high temperature enables high power output, it damages the battery permanently. Available lifetime also decreases under high temperature.

There are four working modes in liquid cooled TMS in GM Volt; heating, bypass, passive, active. The pump always works to circulate coolant. Heating mode uses the heater to increase the coolant temperature when the battery temperature is too low. Bypass mode is on if the battery temperature is just in the optimum range. In this mode, other components except the pump do not works. The pump is the only working component to maintain even temperature distribution inside of the battery pack since the battery generates heat by itself.

Although the temperature is in the optimum range, the radiator works when the temperature goes high. This mode is called passive mode. If the temperature goes higher than the optimum range, the chiller of the air conditioner works to decrease battery temperature fast.

Power consumption of the liquid cooled thermal management system is much higher than one of the air cooled thermal management system. Compared with a fan in the air cooled thermal management system, pump uses much power to circulate liquid state coolant. Heater and chiller in the liquid cooled TMS also use much electric power. Since the electric power consumption of the thermal management system affects battery SOC, an effective control logic that minimizes power consumption but maintains optimum temperature range is needed. Optimal control theories like Pontryagin's minimum principle can be used to develop effective thermal management system control logic. Further studies will be done about this topic.

In this paper, control logic is developed to be matched with experimental data. With the mode change of TMS, the speeds of the pump and the fan in the radiator also change with the battery temperature.

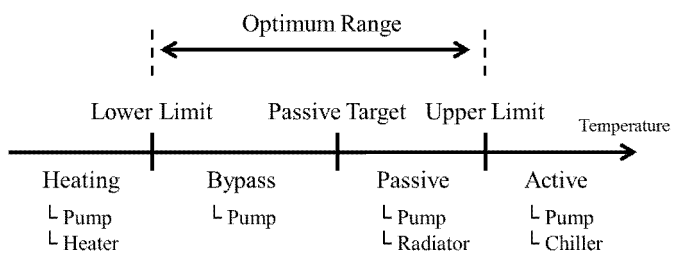

Figure 3.16. Working modes based on the temperature

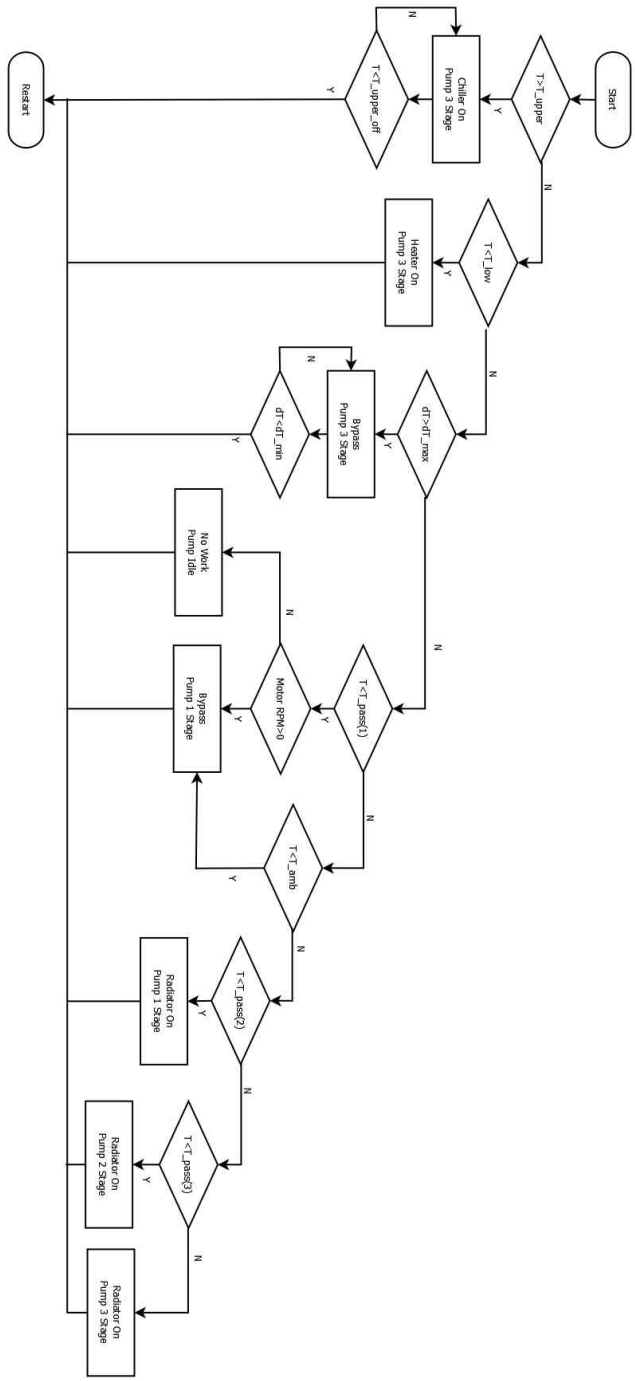

Figure 3.17. Example of liquid cooled TMS control logic

3.2.3. Heat Transfer Theory for Liquid Cooled TMS

Same assumptions about air cooled TMS model are used. Heat transfer between the battery and the coolant can be modeled by using same equations about air cooled TMS model, equation (3.11) and (3.14). Compared with open loop air cooled TMS, liquid cooled TMS uses a closed loop pipe since liquid state coolant is used. Therefore, the outlet coolant temperature becomes the inlet coolant temperature of the next timestep in the simulation. In reality, the outlet coolant has to circulate the closed loop pipe to become the inlet coolant. Time is consumed during the coolant circulation. However, this time consumption is neglected in the simulation due to no time consuming assumption at section 3.1.2.

Modeling heat transfer at the radiator can also be done by the same way as the one at the battery pack. Heat transfer occurs between the ambient air and the coolant. Temperature of the ambient air does not change during whole the time. Coolant temperature changes after passing through radiator. Replacing the battery temperature of equation (3.11) to the ambient air temperature, equation (3.11) can also be used to heat transfer at the radiator.

Heat transfer at the heater is modeled simply by adding the constant amount of heat to the coolant. Power consumption is also modeled as a constant.

$$T_{out} = T_{in} + \frac{Q}{\dot{m} c_{p,cool}} \tag{3.18}$$

In active cooling mode, liquid cooled TMS in GM Volt uses air conditioner to decrease inlet coolant temperature. Heat transfer occurs at the chiller in air conditioner. Heat transfer between two coolant is assumed.

Heat transfer equation about fluid parcel is developed to model heat transfer at the chiller. Coolant 1 is the high temperature TMS coolant and coolant 2 is the low temperature air conditioner coolant. Convection heat transfer occurs between two coolant parcels at the same position.

$$Q = h\big(T_1(x) - T_2(x)\big)dA = h\big(T_1(x) - T_2(x)\big)(Wdx) \tag{3.19}$$

The amount of heat transferred to the coolant 2 fluid parcel from the coolant 1 fluid parcel is same as that of the heat energy decreased when coolant 1 fluid parcel moves to $x+dx$ from x.

$$\dot{m}_1 c_{p,1} T_1(x) = \dot{m}_1 c_{p,1} T_1(x+dx) + Q \tag{3.20}$$

$$\begin{aligned} \therefore Q &= \dot{m}_1 c_{p,1} T_1(x) - \dot{m}_1 c_{p,1} T_1(x+dx) \\ &= h\big(T_1(x) - T_2(x)\big)(Wdx) \end{aligned} \tag{3.21}$$

Equation (3.21) can be rearranged as a differential equation form.

$$-\dot{m}_1 c_{p,1}\big(T_1(x+dx) - T_1(x)\big) = h\big(T_1(x) - T_2(x)\big)(Wdx) \tag{3.22}$$

$$-\dot{m}_1 c_{p,1}\frac{\delta T_1(x)}{\delta x}dx = h\big(T_1(x) - T_2(x)\big)(Wdx) \tag{3.23}$$

$$\therefore \frac{\delta T_1(x)}{\delta x} = \frac{hW}{\dot{m}_1 c_{p,1}}\big(T_2(x) - T_1(x)\big) \tag{3.24}$$

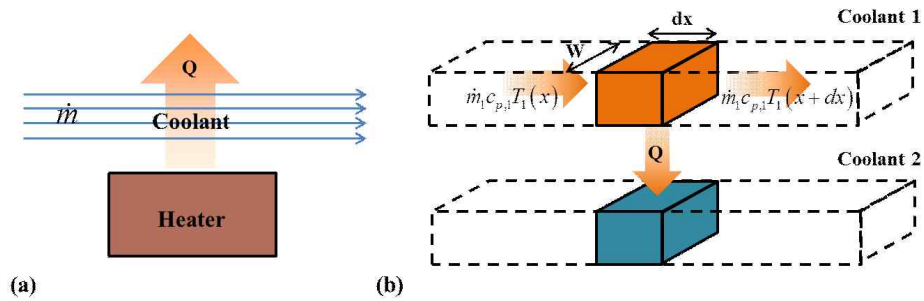

Figure 3.18. Heat transfer mechanism at (a) heater (b) chiller

Similar procedure can be done for the coolant 2 fluid parcel.

$$\frac{\delta T_2(x)}{\delta x} = \frac{h\,W}{\dot{m}_2 c_{p,2}}\left(T_1(x) - T_2(x)\right) \tag{3.25}$$

To solve equation (3.24) and (3.25), equations are changed into matrix form.

$$\begin{aligned}\begin{bmatrix}\frac{dT_1}{dx}\\ \frac{dT_2}{dx}\end{bmatrix} &= \begin{bmatrix}-\frac{h\,W}{\dot{m}_1 c_{p,1}} & \frac{h\,W}{\dot{m}_1 c_{p,1}}\\ \frac{h\,W}{\dot{m}_2 c_{p,2}} & -\frac{h\,W}{\dot{m}_2 c_{p,2}}\end{bmatrix}\begin{bmatrix}T_1\\ T_2\end{bmatrix}\\ &= \begin{bmatrix}-K_1 & K_1\\ K_2 & -K_2\end{bmatrix}\begin{bmatrix}T_1\\ T_2\end{bmatrix}\end{aligned} \tag{3.26}$$

$$\therefore \begin{bmatrix}T_1\\ T_2\end{bmatrix} = \begin{bmatrix}1\\ 1\end{bmatrix}C_1 + \begin{bmatrix}-K_1\\ K_2\end{bmatrix}C_2\exp\{-(K_1+K_2)x\} \tag{3.27}$$

Equation (3.27) can be used for both the counterflow condition ($\dot{m}_1\dot{m}_2 < 0$) and the parallel flow condition ($\dot{m}_1\dot{m}_2 > 0$). Inlet temperatures of two coolants, $T_1(0)$ and $T_2(L)$, become boundary conditions under the counterflow condition. Outlet temperature of coolant 1, $T_1(L)$, can be obtained by solving equation (3.27).

$$\begin{bmatrix}T_1(0)\\ T_2(L)\end{bmatrix} = \begin{bmatrix}1 & -K_1\\ 1 & K_2\exp\{-(K_1+K_2)L\}\end{bmatrix}\begin{bmatrix}C_1\\ C_2\end{bmatrix} \tag{3.28}$$

$$\begin{bmatrix}T_1(L)\\ T_2(0)\end{bmatrix} = \begin{bmatrix}1 & -K_1\exp\{-(K_1+K_2)L\}\\ 1 & K_2\end{bmatrix}\begin{bmatrix}C_1\\ C_2\end{bmatrix} \tag{3.29}$$

If $\dot{m}_1 c_{p,1} + \dot{m}_2 c_{p,2} \neq 0$, following solution can be achieved.

$$\begin{aligned}\begin{bmatrix}T_1(L)\\ T_2(0)\end{bmatrix} &= \frac{1}{K_1 + K_2\exp\{-(K_1+K_2)L\}}\\ &\times\begin{bmatrix}(K_1+K_2)\exp\{-(K_1+K_2)L\} & K_1(1-\exp\{-(K_1+K_2)L\})\\ -K_2(1-\exp\{-(K_1+K_2)L\}) & K_1+K_2\end{bmatrix}\times\begin{bmatrix}T_1(0)\\ T_2(L)\end{bmatrix}\end{aligned} \tag{3.30}$$

Compared with air cooled TMS experimental data, some data of liquid cooled TMS show that the battery temperature rises under no current condition when ambient temperature is higher than the battery pack temperature. It means that direct heat transfer occurs between the battery pack and the ambient air. Fitted thermal resistance value is used to model the heat transfer between the battery pack and the ambient air.

$$Q = (T_{bat} - T_{amb})/R_{th} \tag{3.31}$$

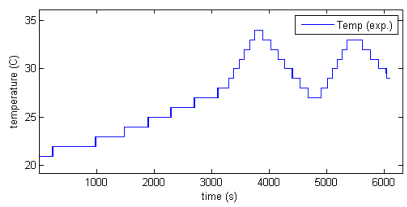

Figure 3.19. Temperature rises under no current, hot ambient condition

3.2.4. Experimental and Simulated Results

Experimental data are given from Hyundai Motor Company, Argonne National Laboratory and SK Innovation. Although experiments were done under vehicle level, simulations were done with battery model only because current loads are given as input data. Experimental data from HMC are summarized in the table 3.5. Each data contains voltage, current, battery temperature, coolant inlet/outlet temperature and mode signals. Data from ANL are similar with HMC. SK Innovation provided on experimental data that mode changes from bypass to passive and active. To validate the simulation model, target temperatures of control logic are changed by using mode signal data of HMC.

Table 3.4. Properties for liquid cooled TMS model

Battery Pack	288 Cells (15Ah each), 197kg
Coolant	50:50 mixture of deionized water and DEX-COOL™
Pump	7L/min, 52W at 100%
Heater	2400W
Radiator	Fan (2ea), 71W at 40%
Chiller	2000W

Table 3.5. HMC experiment data (except error data)

Name	Description
Heater 01	Heating → Bypass
Heater 02	Heating → Bypass
Heater 03	Heating
Passive 01	Bypass → Passive
Passive 03	Bypass → Passive → Bypass
Passive 04	Bypass → Passive → Active → Passive → Active
Active 01	Bypass → Passive → Active
Active 03	Active → Passive → Active
Active 05	Active → Passive

In HMC data, there are some unreasonable components working signals. Heater works at high temperature above 20℃ in Passive 02. Pump signal changes fast under passive mode in Active 03. Signal peaks exist in many experimental data. Most of these behaviors are neglected. Only the outline tendency of control logic change is modeled.

Mode change target temperature appeared to be different between each group. It is thought to be bias error exists in each data. The target temperature in the simulation changed slightly when comparing the simulation data and the experimental data of each group.

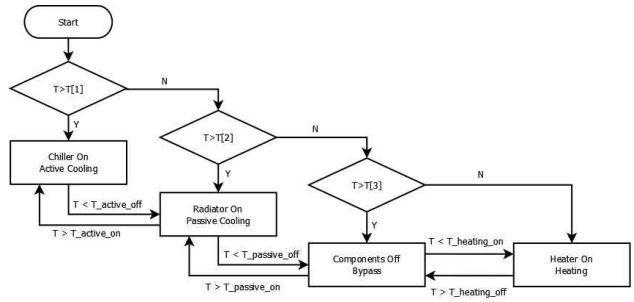

Figure 3.20. Liquid cooled TMS control logic

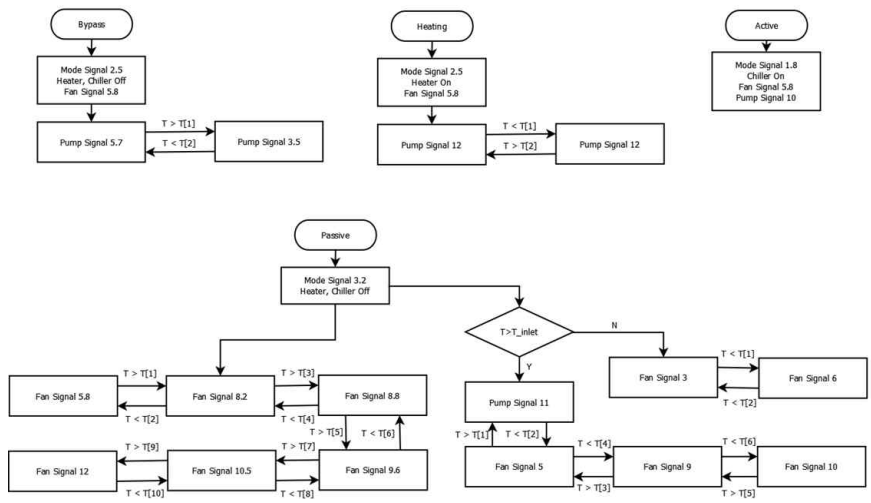

Figure 3.21. Detailed control logic of each mode

The heat transfer coefficient for liquid cooled TMS can be calculated from equations at section 3.1.2. However, it was impossible to calculatr exact value of heat transfer coefficient in this simulation because structure of fins that are inserted between battery cells is not known. Measurement about diameter, length and other properties about the fin is needed to make precise simulation model. Due to the lack of data, assumed heat transfer coefficients are used in the simulation model.

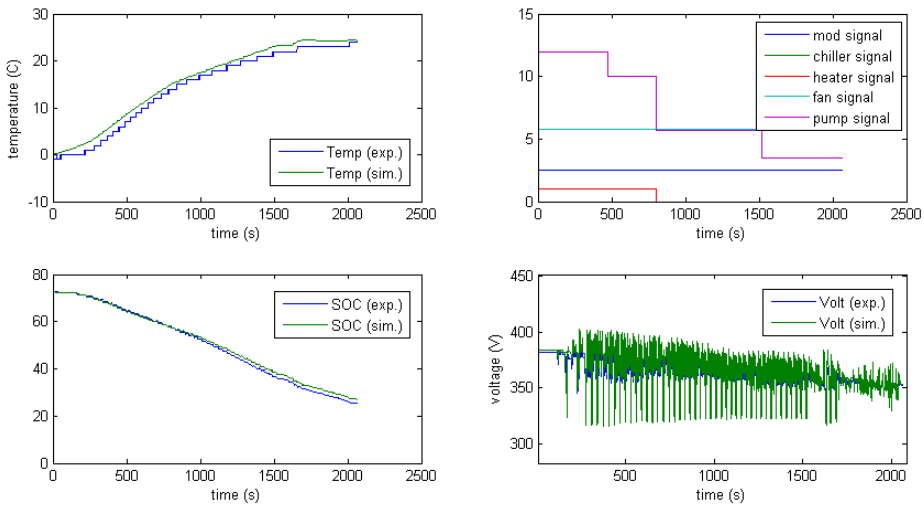

Figure 3.22. Simulation data about HMC Heater 02

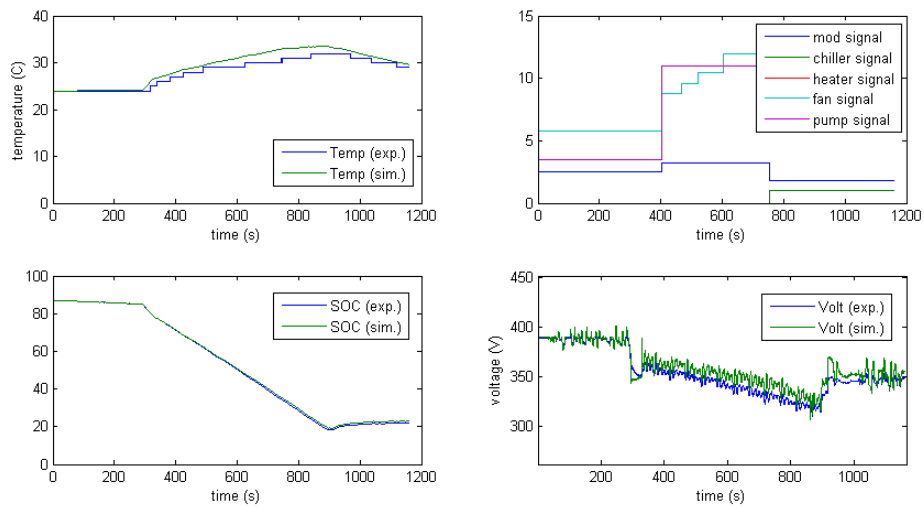

Figure 3.23. Simulation data about HMC Passive 01

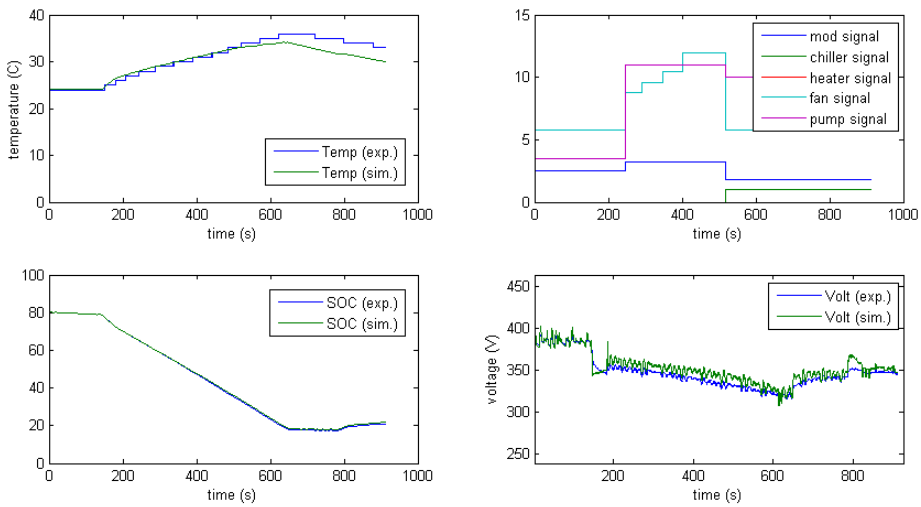

Figure 3.24. Simulation data about HMC Active 01

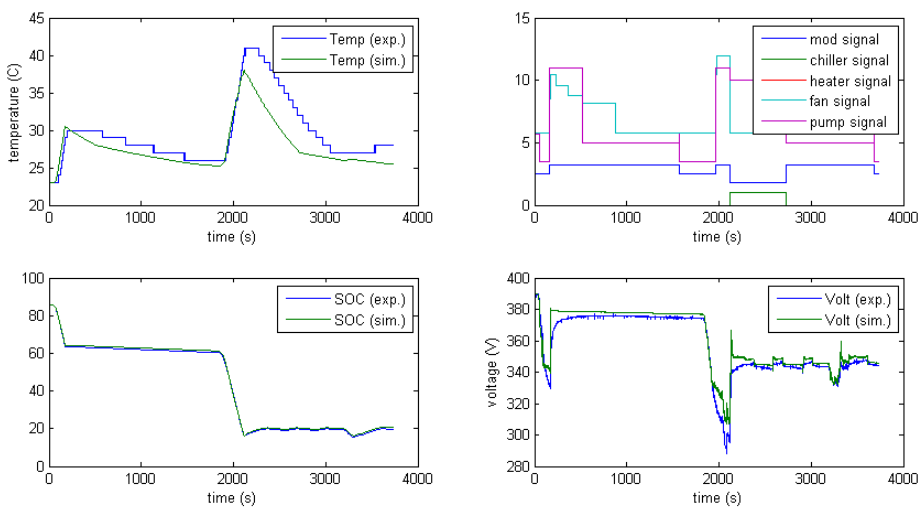

Figure 3.25. Simulation data about SK Innovation data

Simulation data and experimental data match well in most cases. Errors in voltage and SOC are caused by the lack of accuracy in OCV and internal resistance data. The temperature error is caused by many reasons; control logic, heat transfer coefficient, neglected heat transfer phenomena like conduction between battery and vehicle, etc. Also, assumptions that are used can also make errors in simulation results. As mentioned in section 3.1.2, time consumption for coolant flow is neglected in simulation model. These assumptions do not become a problem in air cooled TMS model because ambient air near the inlet is directly drawn to the battery pack and passes though the battery pack fast. Compared to the air cooled thermal management system, liquid state coolant in the liquid cooled thermal management system circulates long pipe. After the coolant passes through the battery pack, it takes a long time that coolant circulates closed loop and turns back as the inlet coolant. Furthermore, remaining coolant exists after the mode change. If mode is changed from passive to active, remaining coolant that passed radiator has to be flow firstly before coolant that passed chiller flows. Time is also consumed until the coolant that passed working components arrives to the battery inlet. To modify errors from these time consumptions, detailed internal structures of the battery pack and the liquid cooled thermal management system have to be known. The lengths of the pipe and the fin are the most important data to model time consumption.

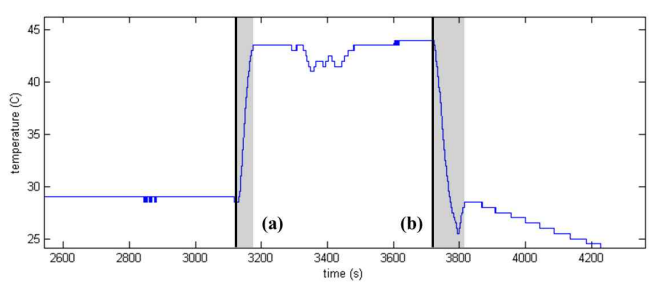

Figure 3.26. Time consumption to change inlet coolant temperature
(a) from bypass to passive (b) from passive to active in HMC Passive 04

4. Battery Capacity Fade Simulation

4.1. Lithium Ion Battery

4.1.1. Lithium Ion Battery Overview

A lithium ion battery is a kind of rechargeable secondary battery that uses lithium ions. It has a high specific energy and a specific power compared with other kinds of batteries. Usable temperature range is also large from under 0℃ to moderate high temperature. Self discharge rate is low and memory effect does not exist [12]. Because of many advantages of the lithium ion battery, it is now used in many applications. Most electric vehicles choose lithium ion batteries as their main power sources in these days. To make vehicles drive for a long time, high energy capacity is needed. High power capacity is also needed to give enough power to the motor under hard condition. The lithium ion battery can satisfy both high energy and high power conditions.

As shown in figure 3.4, the lithium ion battery consists of the positive electrode, the negative electrode and the separator. Lithium ions are intercalated into active materials of each electrode. During discharging, lithium ions inside of the negative electrode are deintercalated and move to the positive electrode. Opposite phenomenon occurs during charging. The electric potential of each electrode change with ion concentration. Temperature and material property also affect the electric potential and the maximum rate of lithium ion intercalation /deintercalation.

Many materials are used to develop a better lithium ion battery [12]. Lithium metal oxides, lithium metal phosphates, lithium sulfur and other materials are used as a positive electrode active material. Lithium cobalt oxide ($LiCoO_2$) and other metal oxides are often used. For the negative electrode, graphite and amorphous carbon are generally used. Electrolyte and additives like binder are also included in electrode.

4.1.2. Capacity Fade of Lithium Ion Battery

Many electrochemical reactions occur inside of the battery. Although major reactions inside of the battery are necessary for battery working, there are some parasitic reactions that make unfavorable effects to the battery. Thermal runaway [13] and gas generation [14] under abuse conditions are related with the battery safety problem. Internal short can occur due to lithium or active material dendrite formation [15]. To make a safe and efficient battery, these parasitic reactions have to be blocked.

The capacity fade of the lithium ion battery is one of the biggest problems to be solved to guarantee a long battery lifetime. Many internal parasitic reactions are related with capacity fade [15-16]. Compared with short changing period of portable devices that use lithium ion batteries, vehicles are used for a longer time. Demanded life of a battery pack in the electric vehicle is long more than 10 years and 1000 cycles [1,17]. Cost of the battery in the electric vehicle is high due to the large size of the battery pack. Therefore, high maintenance cost is needed if the capacity fade of the battery pack is fast.

Capacity fade mechanisms of the lithium ion battery can be separated into

ones at the positive electrode and ones at the negative electrode. Effect of the electrolyte can be handled with the electrode because internal reaction occurs between electrolyte and each electrode. Reactions like corrosion of current collector, decomposition of the binder and the conducting agent can occur at both electrodes. For the positive electrode that uses metal oxides as active materials, structural decomposition or phase change can be reasons of the capacity fade. Many reactions are possible at the positive electrode and most of them are under research. For the graphite negative electrode, solid electrolyte interface, SEI, film generation is considered as a major reason of the capacity fade in many literatures [18-20].

4.2. Simulation Model

4.2.1. General Lithium Ion Battery Model

Porous electrode theory and concentrated solution theory are used for mathematical modeling of the lithium ion battery [21-23]. Early studies were done by Doyle et al [23-27]. Further developments about lithium ion battery models are done based on these battery models [28-31]. Governing equations of 1-D lithium ion battery model used here are summarized in table 4.1. Values for parameters are summarized in table 4.2.

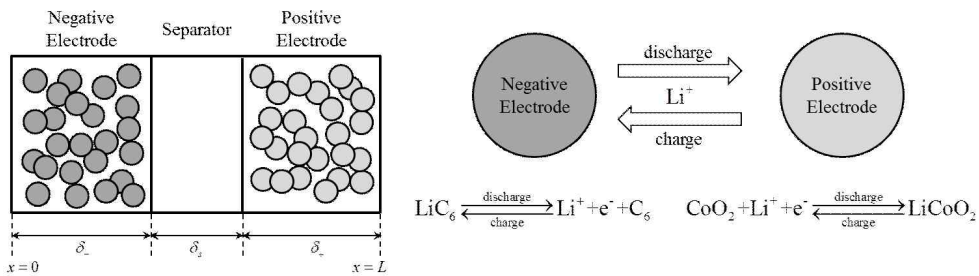

Figure 3.4. Internal reaction of $LiCoO_2/LiC_6$ lithium ion battery (again)

Table 4.1. Governing equations of 1-D lithium ion battery model

Description	Governing equations	Boundary conditions
Potential /Electrolyte	$\frac{\partial \phi_2}{\partial x} = -\frac{i_2}{\kappa_{eff}} + \frac{2RT}{F}\left(1-t_+^0\right)\frac{\partial \ln c}{\partial x}$	$\phi_2\big\vert_{x=L} = 0$ (arbitrary)
Potential /Solid	$I - i_2 = -\sigma_{eff}\frac{\partial \phi_1}{\partial x}$	$i_2\big\vert_{x=0} = i_2\big\vert_{x=L} = 0$ $i_2\big\vert_{x=\delta_-} = i_2\big\vert_{x=\delta_- + \delta_s} = I$ (galvanostatic condition)
Transport /Electrolyte	$\epsilon\frac{\partial c}{\partial t} = \frac{\partial}{\partial x}\left(D^{eff}\frac{\partial c}{\partial x}\right) + \frac{1-t_+^0}{F}\frac{\partial i_2}{\partial x}$	$\left.\frac{\partial c}{\partial x}\right\vert_{x=0} = \left.\frac{\partial c}{\partial x}\right\vert_{x=L} = 0$
Transport /Solid	$\frac{\partial c_s}{\partial t} = \frac{1}{r^2}\frac{\partial}{\partial r}\left(D_s r^2 \frac{\partial c_s}{\partial r}\right)$	$\left.\frac{\partial c_s}{\partial r}\right\vert_{r=0} = 0$ $-D_s\left.\frac{\partial c_s}{\partial r}\right\vert_{r=R_s} = j_{Li}$ initial condition: $c_s(t=0,x,r) = c_s^0$
Reaction rate	$i_n = i_0\left[\exp\left(\frac{\alpha_a F(\phi_1 - \phi_2 - U)}{RT}\right) - \exp\left(\frac{-\alpha_c F(\phi_1 - \phi_2 - U)}{RT}\right)\right]$	
Exchange current density	$i_0 = F(k_a)^{\alpha_c}(k_c)^{\alpha_a}(c_{s,\max} - c_s)^{\alpha_c}(c_s)^{\alpha_a}(c)^{\alpha_a}$	
Current balance	$\frac{\partial i_2}{\partial x} = a i_n$ $j_{Li} = \frac{i_n}{F}$	$i_n\big\vert_{x=\delta_- \sim \delta_- + \delta_s} = 0$
Voltage	$V = \phi_1\big\vert_{x=L} - \phi_1\big\vert_{x=0}$	
Effective properties	$D^{eff} = D\epsilon^p$ $\kappa^{eff} = \kappa\epsilon^p$ $\sigma^{eff} = \sigma\epsilon_s$ $a = \frac{3\epsilon_s}{R_s}$	

Table 4.2. Parameters for simulation

Parameter	Units	Negative electrode	Separator	Positive electrode
		Graphite	LiPF6 in 2:1 EC/DMC and p(VDF-HFP)	$LiCoO_2$
δ	m	88×10^{-6}	25×10^{-6}	80×10^{-6}
R_s	m	2×10^{-6}		2×10^{-6}
ϵ		0.485	0.724	0.385
ϵ_s		0.49		0.59
$c_{s,\max}$	mol/m^3	30555		51555
$c_{s,0}$	mol/m^3	0.8551×30555		0.4955×51555
c_0	mol/m^3	1000	1000	1000
k_a	$m/s\cdot(mol/m^3)^{\alpha_a}$	5.0307×10^{-11}		2.334×10^{-11}
k_c	$m/s\cdot(mol/m^3)^{\alpha_a}$	5.0307×10^{-11}		2.334×10^{-11}
α_a		0.5		0.5
α_c		0.5		0.5
D_s	m^2/s	3.9×10^{-14}		1.0×10^{-14}
σ	S/m	100		100
D	m^2/s	7.5×10^{-10}	7.5×10^{-10}	7.5×10^{-10}
p		4.0	4.0	4.0
t_+^0			0.363	
Area	m^2		0.030	
κ	S/m	$4.1252\times10^{-2}+5.007\times10^{-4}c-4.7212\times10^{-7}c^2+1.5094\times10^{-10}c^3-1.6018\times10^{-14}c^4$		
U	V	$U_n=0.7222+0.13870\theta_n+0.029\theta_n^{0.5}-\frac{0.0172}{\theta_n}+\frac{0.0019}{\theta_n^{1.5}}+0.2808\exp(0.90-15\theta_n)-0.7984\exp(0.4465\theta_n-0.4108)$		
		$U_p=\frac{-4.656+88.669\theta_p^2-401.119\theta_p^4}{-1.0+18.933\theta_p^2-79.532\theta_p^4}+\frac{+342.909\theta_p^6-462.471\theta_p^8+433.434\theta_p^{10}}{+37.311\theta_p^6-73.083\theta_p^8+95.96\theta_p^{10}}$ where $\theta=c_s\big\vert_{r=R_s}/c_{s,\max}$		

* most values are from reference [30-31]

To solve the coupled partial differential equations at table 4.1, numerical schemes are used. Partial differential equations about x-direction can be changed into a finite differential form with accuracy $O(h^2)$.

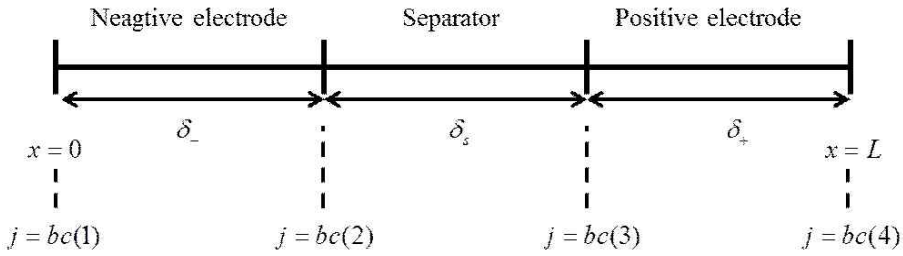

Figure 4.1. Grid in x-direction

Table 4.3. Governing equations at each grid

$g_1(x)$	Potential/Electrolyte
	$j = bc(1) \sim bc(4) - 1$ $g_1(x) = \frac{\partial \phi_2}{\partial x} + \frac{i_2}{\kappa_{eff}} - \frac{2RT}{F}(1 - t_+^0)\frac{\partial \ln c}{\partial x} = 0$
	$j = bc(4)$ $g_1(x) = \phi_2 \vert_{x=L} = 0$
$g_2(x)$	Potential/Solid
	$j = bc(1)$ $g_2(x) = i_2 \vert_{x=0} = 0$
	$j = bc(1) + 1 \sim bc(2)$ $g_2(x) = \sigma_{eff}\frac{\partial \phi_1}{\partial x} - i_2 + I = 0$
	$j = bc(2) + 1 \sim bc(3)$ $g_2(x) = i_2 - I = 0$
	$j = bc(3) + 1 \sim bc(4)$ $g_2(x) = \sigma_{eff}\frac{\partial \phi_1}{\partial x} - i_2 + I = 0$
$g_3(x)$	Reaction rate
	$j = bc(1) \sim bc(2)$ $g_3(x) = i_n - i_0\left[\exp\left(\frac{\alpha_a F(\phi_1 - \phi_2 - U)}{RT}\right) - \exp\left(\frac{-\alpha_c F(\phi_1 - \phi_2 - U)}{RT}\right)\right] = 0$
	$j = bc(2) + 1 \sim bc(3) - 1$ $g_3(x) = \phi_1 = 0$

	$j = bc(3) \sim bc(4)$
	$g_3(x) = i_n - i_0\left[\exp\left(\frac{\alpha_a F(\phi_1 - \phi_2 - U)}{RT}\right) - \exp\left(\frac{-\alpha_c F(\phi_1 - \phi_2 - U)}{RT}\right)\right] = 0$
$g_4(x)$	Current Balance
	$j = bc(1) \sim bc(2) - 1$
	$g_4(x) = \frac{\partial i_2}{\partial x} - a i_n = 0$
	$j = bc(2)$
	$g_4(x) = i_2 - I = 0$
	$j = bc(2) + 1 \sim bc(3) - 1$
	$g_4(x) = i_n = 0$
	$j = bc(3) \sim bc(4) - 1$
	$g_4(x) = \frac{\partial i_2}{\partial x} - a i_n = 0$
	$j = bc(4)$
	$g_4(x) = i_2\big\vert_{x=L} = 0$

Newton-Raphson method for block tridiagonal matrix is used for the equations in table 4.3 [21]. Block PLU decomposition is also used. Solution for the each timestep can be achieved by iterative solver. Compared with the equations about x-direction, the partial differential equations about transport can be solved by Crank-Nicolson method. For the internal boundaries, the control volume method is used [23]. With the results of the iterative solver, it is possible to obtain the time dependent solution of the coupled partial differential equations.

4.2.2. Capacity Fade Model with Temperature Effect

Capacity fade due to SEI film generation is frequently chosen for the major reason of the capacity fade in the lithium ion battery simulation [30,32-39]. Although SEI film has to be generated once between the electrode and the

electrolyte interface, SEI film stretches due to gas generation [40] or lattice volume change [41] of the graphite negative electrode. Cracks occur in the film. Therefore, lithium ions and solvent molecules can go through the cracks and react with exposed carbon. SEI film becomes thicker because of this reaction. Composition of SEI film depends on the type of solvent. For ethylene carbonate, EC, or dimethyl carbonate, DMC, [42]

$$2(CH_2O)_2CO\ (EC) + 2e^- + 2Li^+ \rightarrow (CH_2OCO_2Li)_2 \downarrow + C_2H_4 \uparrow \quad (4.1)$$

$$CH_3OCO_2CH_3\ (DMC) + e^- + Li^+ \rightarrow CH_3OCO_2Li \downarrow + CH_3 \quad (4.2)$$

This kind of irreversible cathodic reaction can be modeled as Tafel equation. As results of SEI film generation, lithium ions are consumed and internal resistance increases. These phenomena affect to the battery capacity fade.

Table 4.4. New and modified equations for capacity fade simulation

Description	Governing equations	Boundary conditions
Reaction rate for SEI film	$i_{para} = -i_{0,para}\exp\left(\frac{-\alpha_{c,para}F\{\phi_1-\phi_2-U_{para}-(i_n+i_{para}))R_{film}\}}{RT}\right)$	
Reaction rate	$i_n = i_0\left[\exp\left(\frac{\alpha_a F\{\phi_1-\phi_2-U-(i_n+i_{para}))R_{film}\}}{RT}\right) - \exp\left(\frac{-\alpha_c F\{\phi_1-\phi_2-U-(i_n+i_{para}))R_{film}\}}{RT}\right)\right]$	
Current Balance	$\frac{\partial i_2}{\partial x} = a(i_n+i_{para})$ $j_{Li} = \frac{i_n}{F}$	$i_n\big\vert_{x=\delta_- \sim \delta_- + \delta_s} = 0$ $i_{para}\big\vert_{x=\delta_- \sim \delta_- + \delta_s + \delta_+} = 0$
Film resistance	$\frac{\partial \delta_{film}}{\partial t} = -\frac{i_{para} \times M_{film}}{\rho_{film} \times F}$ $R_{film} = \frac{\delta_{film}}{\kappa_{film}}$	$\delta_{film}(x, t=0) = 0$
Capacity fade	$i_s = \int_0^{\delta_-} a i_{para} dx$ $Q_s = \int_0^t i_s dt$	Total capacity : $Q = \int_0^t I dt$

Table 4.5. Parameters for capacity fade simulation

Parameter	Units	EC decomposition at negative elctrode
U_{para}	V	0.38
$i_{0,para}$	A/m^2	8×10^{-8}
$\alpha_{c,para}$		0.5
M_{film}	kg/mol	0.1
ρ_{film}	kg/m^3	2.1×10^{3}
κ_{film}	S/m	3.79×10^{-7}

* most values are from reference [35-36]

Reactions that occured inside of the battery are affected by the temperature. Properties like diffusivity [43-45], conductivity [46-47] and exchange current density [48] change with the temperature. Open circuit voltage also changes because of the Nernst equation. Butler-Volmer equation for the reactions rate contains temperature terms. Since the temperature affects internal reactions, the performance of the battery changes with the temperature [1,48-49].

The Speed of the capacity fade is also affected by the temperature. [2-3,18,49]. To adapt temperature effect to the capacity fade model, Arrhenius equation is used for the exchange current density of SEI film generation. Because of the insufficient experimental data, the activation energy for the exchange current density of the film generation is assumed as $25kJ/mol$.

Table 4.6. Temperature effect for the SEI film generation

Description	Equation	Conditions
Exchange current density for SEI film generation	$i_{0,para} = Aexp\left(-\frac{E_{a,para}}{RT}\right)$	$E_{a,para} = 25kJ/mol$ $i_{0,para} = 8\times10^{-8}A/m^2$ $at\ 25℃$

4.2.3. Simplified Battery Models

Beside the general lithium ion battery model, two types of simplified battery models are simulated; single particle model and Randles circuit model.

Single particle model assumes each electrode as single spherical particle. Potential gradient and concentration gradient along the current path are neglected inside of each electrode [50-52]. Diffusion at each spherical particle is calculated by Firck's law. Using a single particle assumption, equation about the voltage can be simplified.

$$V = OCV + \frac{2RT}{F}\ln\left(\frac{\sqrt{m_p^2+4}-m_p}{2}\right) + \frac{2RT}{F}\ln\left(\frac{\sqrt{m_n^2+4}-m_n}{2}\right) - IR \qquad (4.3)$$
$$\text{where } m = \frac{I}{FkSc_{s,\max}c_e^{0.5}(1-x_{surf})^{0.5}x_{surf}^{0.5}}$$

This model is used for the battery model in the thermal management system model. Surface lithium concentration is needed to calculate the voltage of the battery. At the thermal management system model, SOC is assumed as the surface lithium concentration ratio.

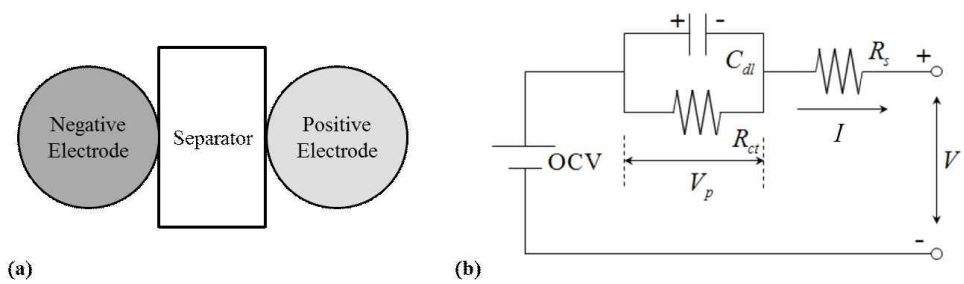

Figure 4.2. (a) Single particle model (b) Randles circuit model

Randles circuit model simply uses an electrical equivalent circuit. This model is often used to analyse the impedance values measured from electrochemical impedance spectroscopy [48]. Randles circuit for the battery model often consists of internal resistance due to separator (R_s), charge transfer resistance (R_{ct}) and double layer capacitance (C_{dl}).

$$V = OCV - V_p - IR_s$$
$$\text{where } \frac{dV_p}{dt} = -\frac{1}{R_{ct}C_{dl}}V_p + \frac{1}{C_{dl}}I \tag{4.4}$$

Simulations are done by using both models about one battery cell under the natural convection condition. Both battery models show almost same result. Voltage mismatch occurs two times. The first mismatch occurs when SOC becomes higher than 1 in the experimental result. SOC value of the simulation model has an upper bound near 1. Therefore, voltage mismatch occurred due to the difference between SOC. The second mismatch is occurred at the pulse current region. This mismatch appears due to the lack of accuracy in simulation model. Simulation time for Randles circuit model is shorter than single particle model. However, single particle model has advantages that importing side reactions like capacity fade is possible.

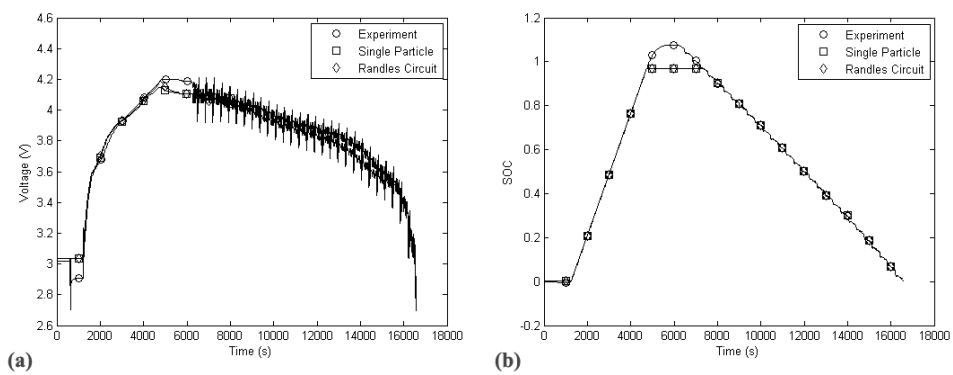

Figure 4.3. Simulation data about two simulation models (a) voltage (b) SOC

4.3. Simulation Results

Capacity fade simulation was done by using general battery model. 30Ah/m^2 $LiCoO_2/LiPF_6/LiC_6$ was chosen. Half C-rate constant current (CC) discharging until 3.0V and half C-rate CC charging until 4.2V was done. When the voltage reaches 4.2V, constant voltage (CV) charging was done until the current reaches 0.05A/m^2. This cycle repeated 2500 times. Simulated time is about 527 days. Initial 30Ah/m^2 capacity decreased to nearly 20Ah/m^2 after 2500 cycles. For 1000 cycles, demanded life for ethe lectric vehicle battery pack [1,17], capacity becomes about 83% of initial value. Therefore, it is possible to say that this battery cell is suitable for electric vehicles.

Before the temperature effect for the battery capacity fade is simulated, some constants about SEI film generation are changed to make the fast simulation possible. $i_{0,para}$ is changed to $1.5\times10^{-6}A/m^2$ at 25℃ and κ_{film} becomes $1.0\,S/m$. The capacity fade becomes about 20 times faster in this case. By adapting temperature effect to the simulation, it is possible to show that high temperature accelerates the capacity fade of the battery.

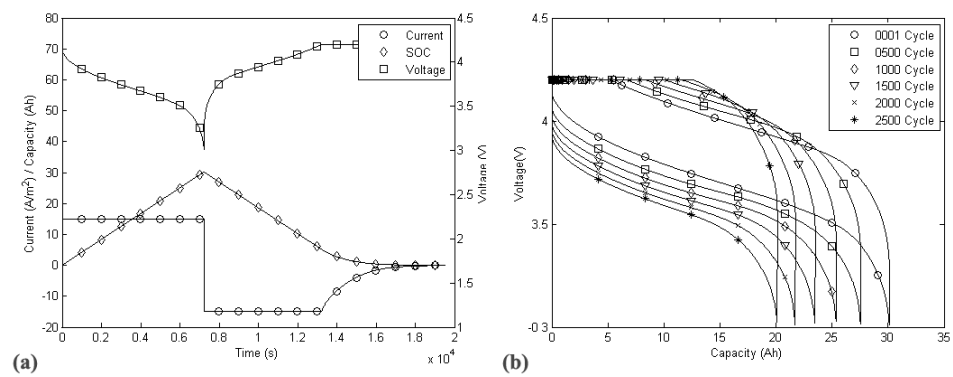

Figure 4.4. Simulation data about (a) first cycle (b) 2500 cycle

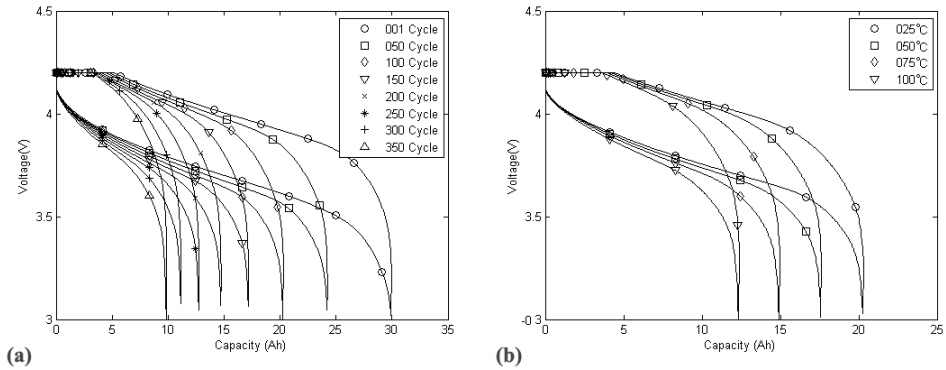

Figure 4.5. Fast simulation data about (a) 350 cycle (b) temperature change

5. Conclusion

5.1. Conclusion

In this thesis, the thermal management system and the capacity fade model for a lithium ion battery are developed and simulated. In chapter 3, both the air cooled and the liquid cooled thermal management systems are modeled under heat transfer theories. Fitting factors are used for heat transfer coefficients. Simulated results and experimental results match well in most cases. However, due to the assumptions that are used, some mismatch points are found.

The thermal managements system model can be used to find the most efficient battery pack arrangement for the air cooled thermal management system. As shown in chapter 3.1.5, the maximum temperature and the temperature difference inside of the battery pack change with the pack arrangement. By using simulation results to designing a thermal management system, it will helps to make safe and efficient battery operation possible.

The capacity fade of lithium ion battery is simulated in chapter 4. Simulation results shows 17% of capacity fade after 1000 CC-CV cycle, which is enough for an electric vehicle battery pack. However, capacity fade simulated here is only caused by SEI film generation. In reality, many other side reactions affect capacity fade. To simulate the battery capacity fade correctly, knowledge about the side reactions is important.

High temperature accelerates the capacity fade because side reactions are activated at high temperature. By using thermal management system to make

the battery temperature lower, it will be possible to decrease capacity fade of the battery pack. Since thermal management system uses battery power for working, the proper control logic that minimizes the capacity fade and the power consumption is important.

5.2. Future Works

Following topics will be covered in future studies.

- Importing battery capacity fade model into the thermal management system model to show effect of thermal management system for capacity fade.
- Developing proper thermal management system control logic.
- Finding proper values for battery model to minimize error.
- Simulating temperature effect to the capacity fade under non-accelerated condition.
- Simulating battery capacity fade by other methods like aging property.

References

[1] Roland Matthe, Lance Turner, Horst Mettlach, "VOLTEC Battery System for Electric Vehicle with Extended Range", SAE International Journal of Engines, 4, 1, 2011.

[2] I. Bloom, B.W. Cole, J.J. Sohn, S.A. Jones, E.G. Polzin, V.S. BAttaglia, G.L. Henriksen, C. Motloch, R. Richardson, T. Unkelhaeuser, D. Ingersoll, H.L. Case, “An accelerated calendar and cycle life study of Li-ion cells”, Journal of Power Sources, 101, 2, 2001.

[3] Tao Zheng, Antoni S. Gozdz, Glenn G. Amatucci, "Reactivity of the Solid Electrolyte Interface on Carbon Electrodes at Elevated Temperatures", Journal of The Electrochemical Society, 146, 11, 1999.

[4] Ahmad A. Pesaran, "Battery thermal models for hybrid vehicle simulations", Journal of Power Sources, 110, 2, 2002.

[5] Gi-Heon Kim, Ahmad A. Pesaran, "Battery Thermal Management System Design Modeling", 22nd International Battery, Hybrid and Fuel Cell Electric Vehicle Conference and Exhibition, Yokohama, Japan, October 23-28, 2006.

[6] Ahmad A. Pesaran, Andreas Vlahinos, Thomas Stuart, "Cooling and Preheating of Batteries in Hybrid Electric Vehicles", The 6th ASME-JSME Thermal Engineering Joint Conference, Hawaii, USA, March 16-20, 2003.

[7] Zhonghao Rao, Shuangfeng Wang, "A review of power battery thermal energy management", Renewable and Sustainable Energy Reviews, 15, 9, 2011.

[8] Frank P. Incropera, David P. Dewitt, Theodore L. Bergman, Adrienne S. Lavine, “Fundamentals of Heat and Mass Transfer”, 6e, Wiley, 2007.

[9] Robert Parrish, Kanthasamy Elankumaran, Milind Gandhi, Bryan Nance, Patrick Meehan, Dave Milburn, Saif Siddiqui, Andrew Brenz, "Voltec Battery Design and Manufacturing", SAE Technical Paper, 2011.

[10] “2013 Chevrolet Volt Owner Manual”, General Motors, 2013.

[11] Keith Buford, Jonathan Williams, Matthew Simonini, "Determining Most Energy Efficient Cooling Control Strategy of a Rechargeable Energy Storage System", SAE Technical Paper, 2011.

[12] P Kurzweil, K Barndt, “SECONDARY BATTERIES – LITHIUM RECHARGEABLE SYSTEMS: Overview”, Encyclopedia of Electrochemical Power Sources, 2009.

[13] Shin-ichi Tobishima, Koji Takei, Yoji Sakurai, Jun-ichi Yamaki, "Lithium ion cell safety", Journal of Power Sources, 90, 2, 2000.

[14] Kazuma Kumai, Hajime Miyashiro, Yo Kobayashi, Katsuhito Takei, Rikio Ishikawa, "Gas generation mechanism due to electrolyte decomposition in commercial lithium-ion cell", Journal of Power Sources, 81-82, 1, 1999.

[15] Pankaj Arora, Ralph E. White, Marc Doyle, "Capacity Fade Mechanisms and Side Reactions in Lithium-Ion Batteries", Journal of The Electrochemical Society, 145, 10, 1998.

[16] J. Vetter, P. Novák, M.R. Wagner, C. Veit, K.-C. Möller, J.O. Besenhard, M. Winter, M. Wohlfahrt-Mehrens, C. Vogler, A. Hammouche, "Ageing mechanisms in lithium-ion batteries", Journal of Power Sources, 147, 1-2, 2005.

[17] "Energy Storage System Goals: USABC Goals for Advanced Batteries for EVs", United States Advanced Battery Consortium, 2006.

[18] M. Broussely, S. Herreyre, P. Biensan, P. Kasztejna, K. Nechev, R. J. Staniewicz, "Aging mechanism in Li ion cells and calendar life predictions", Journal of Power Sources, 97-98, 1, 2001.

[19] Yoshinori Kida, Akira Kinoshita, Katsunori Yanagida, Atsuhiro Funahashi, Toshiyuki Nohma, Ikuo Yonezu, "Study on capacity fade factors of lithium secondary batteries using LiNi0.7Co0.3O2 and graphite-coke hybrid carbon", Electrochimica Acta, 47, 1, 2002.

[20] Doron Aurbach, Ella Zinigrad, Yaron Cohen, Hanan Teller, "A short review of failure mechanisms of lithium metal and lithiated graphite anodes in liquid electrolyte solutions", Solid State Ionics, 148, 1, 2002.

[21] John Newman, Karen E. Thomas-Alyea, "Electrochemical Systems", 3e, Wiley, 2004.

[22] Karen E. Thomas, John Newman, Robert M. Darling, “Mathematical Modeling of Lithium Batteries”, Advances in Lithium-Ion Batteries, 2002.

[23] C.M. Doyle, "Design and Simulation of Lithium Rechargeable Batteries", Ph.D. Thesis, University of California, Berkeley, 1995.

[24] Marc Doyle, Thomas F. Fuller, John Newman, "Modeling of Galvanostatic Charge and Discharge of the Lithium/Polymer/Insertion Cell", Journal of The Electrochemical Society, 140, 6, 1993.

[25] Thomas F. Fuller, Marc Doyle, John Newman, "Simulation and Optimization of the Dual Lithium Ion Insertion Cell", Journal of The Electrochemical Society, 141, 1, 1994.

[26] Thomas F. Fuller, Marc Doyle, John Newman, "Relaxation Phenomena in Lithium-Ion-Insertion Cells", Journal of The Electrochemical Society, 141, 4, 1994.

[27] Marc Doyle, John Newman, "Comparison of Modeling Predictions with Experimental Data from Plastic Lithium Ion Cells", Journal of The Electrochemical Society, 143, 6, 1996.

[28] Kandler Smith, Chao-Yang Wang, "Power and thermal characterization of a lithium-ion battery pack for hybrid-electric vehicles", Journal of Power Sources, 160, 1, 2006.

[29] Shriram Santhanagopalan, Qingzhi Guo, Premanand Ramadass, Ralph E. White, "Review of models for predicting the cycling performance of lithium ion batteries", Journal of Power Sources, 156, 1, 2006.

[30] P. Ramadass, Bala Haran, Parthasarathy M. Gomadam, Ralph White, Branko N. Popov, "Development of First Principles Capacity Fade Model for Li-Ion Cells", Journal of The Electrochemical Society, 151, 2, 2004.

[31] Venkat R. Subramanian, Vijayasekaran Boovaragavan, Venkatasailanathan Ramadesigan, Mounika Arabandi, "Mathematical Model Reformulation for Lithium-Ion Battery Simulations: Galvanostatic Boundary Conditions", Journal of The Electrochemical Society, 156, 4, 2009.

[32] R. Spotnitz, "Simulation of capacity fade in lithium-ion batteries", Journal of Power Sources, 113, 1, 2003.

[33] P. Ramadass, Bala Haran, Ralph White, Branko N. Popov, "Mathematical modeling of the capacity fade of Li-ion cells", Journal of Power Sources, 134, 1, 2003.

[34] J. Christensen, J. Newman, "Effect of Anode Film Resistance on the Charge/Discharge Capacity of a Lithium-Ion Battery", Journal of The Electrochemical Society, 150, 11, 2003.

[35] Gang Ning, Branko N. Popov, "Cycle Life Modeling of Lithium-Ion Batteries", Journal of The Electrochemical Society, 151, 10, 2004.

[36] Gang Ning, Ralph E. White, Branko N. Popov, "A generalized cycle life model of rechargeable Li-ion batteries", Electrochimica Acta, 51, 10, 2006.

[37] M. Safari, M. Morcrette, A. Teyssot, C. Delacourt, "Multimodal Physics-Based Aging Model for Life Prediction of Li-Ion Batteries", Journal of The Electrochemical Society, 156, 3, 2009.

[38] Ali Awarke, Stefan Pischinger, Jürgen Ogrzewalla, "Pseudo 3D Modeling and Analysis of the SEI Growth Distribution in Large Format Li-Ion Polymer Pouch Cells", Journal of The Electrochemical Society, 160, 1, 2013.

[39] Matthew B. Pinson, Martin Z. Bazant, "Theory of SEI Formation in Rechargeable Batteries: Capacity Fade, Accelerated Aging and Lifetime Prediction", Journal of The Electrochemical Society, 160, 2, 2013.

[40] Gang Ning, Bala Haran, Branko N. Popov, "Capacity fade study of lithium-ion batteries cycled at high discharge rates", Journal of Power Sources, 117, 1-2, 2003.

[41] Doron Aurbach, "Review of selected electrode‐solution interactions which determine the performance of Li and Li ion batteries", Journal of Power Sources, 89, 2, 2000.

[42] A.M. Andersson, M. Herstedt, A.G. Bishop, K. Edström, "The influence of lithium salt on the interfacial reactions controlling the thermal stability of graphite anodes", Electrochimica Acta, 47, 23, 2002.

[43] A. Van der Ven, G. Ceder, "Lithium Diffusion in Layered LixCoO2", Electrochemical and Solid-State Letters, 3, 7, 2000.

[44] Kisuk Kang, Ying Shirley Meng, Julien Bréger, Clare P. Grey, Gerbrand Ceder, "Electrodes with High Power and High Capacity for Rechargeable Lithium Batteries", Science, 311, 1, 2006.

[45] Kazuaki Toyoura, Yukinori Koyama, Akihide Kuwabara, Isao Tanaka, "Effects of Off-Stoichiometry of LiC6 on the Lithium Diffusion Mechanism and Diffusivity by First Principles Calculations", 114, 5, 2010.

[46] Janina Molenda, Andrzej Stoklosa, Tadeusz Bąk, "Modification in the electronic structure of cobalt bronze LixCoO2 and the resulting electrochemical properties", Solid State Ionics, 36, 1-2, 1989.

[47] M. S. Ding, K. Xu, S. S. Zhang, K. Amine, G. L. Henriksen, T. R. Jow, "Change of Conductivity with Salt Content, Solvent Composition, and Temperature for Electrolytes of LiPF6 in Ethylene Carbonate-Ethyl Methyl Carbonate", Journal of The Electrochemical Society, 148, 10, 2001.

[48] Masaya Takahashi, Shin-ichi Tobishima, Koji Takei, Yoji Sakurai, "Reaction behavior of LiFePO4 as a cathode material for rechargeable lithium batteries", Solid State Ionics, 148, 3-4, 2002.

[49] Honghe Zheng, Jianhua Qin, Yang Zhao, Takeshi Abe, Zempachi Ogumi, "Temperature dependence of the electrochemical behavior of LiCoO2 in quaternary ammonium-based ionic liquid electrolyte", Solid State Ionics, 176, 29-30, 2005.

[50] Gang Ning, Branko N. Popov, "Cycle Life Modeling of Lithium-Ion Batteries", Journal of The Electrochemical Society, 151, 10, 2004.

[51] Shriram Santhanagopalan, Qingzhi Guo, Premanand Ramadass, Ralph E. White, "Review of models for predicting the cycling performance of lithium ion batteries", Journal of Power Sources, 156, 2, 2006.

[52] Meng Guo, Godfrey Sikha, Ralph E. White, "Single-Particle Model for a Lithium-Ion Cell: Thermal Behavior", Journal of The Electrochemical Society, 158, 2, 2011.

국문초록

전기차용 리튬 이온 배터리 열관리 시스템 모델 및 용량 저하 모델 개발

최종우

기계항공공학부

대학원

서울대학교

전기자동차에 들어가는 리튬 이온 배터리를 위한 열관리 시스템 모델을 구현하였다. 대류 열전달 이론을 사용하여 공랭식/수랭식 각 타입의 열관리 시스템을 구현하였으며, 시뮬레이션 결과와 실험 결과의 비교가 이루어졌다. OCV와 내부 저항은 실험값을 온도와 SOC에 따른 맵으로 변환하여 모델에 삽입하였으며, activation loss를 구현하기 위해 필요한 상수들은 문헌 값을 사용하였다. 시뮬레이션 결과는 일부 문제가 되는 부분들이 존재하였지만 전체적으로 낮은 오차 범위 내에서 일치하는 것이 확인되었다. 시뮬레이션 모델을 사용하여 공랭식 시스템에서 최적의 효과를 낼 수 있는 배터리 팩 배열 방식을 확인하는 것이 가능하였으며, 이는 안전과 효율 두 측면에서 도움이 될 것으로 예상된다.

리튬 이온 배터리의 용량 저하 현상에 대한 모델 또한 구현되었으며, SEI 필름 형성에 따른 용량 저하 현상을 기반으로 하여 구현이 이루어졌다. 시뮬레이션 결과 온도가 용량 저하에 영향을 준다는 것이 확인되었으며, 높은 온도일수록 용량 저하 속도가 빠르다는 것이 확인되었다. 이 배터리 모델을 앞서 개발한 열관리 시스템 모델에 탑재할 경우 배터리의

SOH를 증대시키면서도 효율적인 작동이 가능한 열관리 시스템 작동 로직 개발에 도움이 될 것으로 예상된다.

주요어 : 리튬 이온 배터리, 전기자동차, 열관리 시스템, 용량 저하, State of Health

학 번 : 2011-20764